Nuclear Engineering and Design 418 (2024) 112840

Contents lists available at ScienceDirect

Nuclear Engineering and Design

journal homepage: www.elsevier.com/locate/nucengdes

Validation of the dynamic simulation capabilities of Serpent2/Subchanflow using experimental data from the research reactor SPERT IV D-12/25

Juan Carlos Almachi [a], Victor Sánchez-Espinoza [a,*], Uwe Imke [a], Robert Stieglitz [a], Marat Margulis [b]

[a] Karlsruhe Institute of Technology, Institute for Neutron Physics and Reactor Technology, Hermann-von-Helmholtz-Platz 1, D-76344 Eggenstein-Leopoldshafen, Germany

[b] Nuclear Futures Institute, School of Computer Science and Electronic Engineering, Bangor University, Bangor LL57 2DG, UK

ARTICLE INFO

Keywords:
Serpent2/Subchanflow
Transient analysis
SPERT IV
Validation
High-fidelity
MTR-cores

ABSTRACT

Research nuclear reactors are critical to the development of nuclear technology, but because of the complex configuration of the fuel assemblies and the different initial operating conditions, neutronic and thermal–hydraulic analyzes are performed with dedicated or adapted codes. These simulation tools might not be as accurate, since they use simple resolution methods and assumptions that do not always capture all aspects of the behavior of a nuclear research reactor. On the other hand, as time goes by, the evolution of numerical tools for the core analysis of power reactors have experienced a considerable progress. Nowadays, pin/subchannel level analysis of the core with coupled codes based on transport (SP3, MOC, SN, etc.) or Monte Carlo methods are applied in addition to the nodal diffusion codes. Hence, the research community is adapting and validating selected high-fidelity tools developed for power reactors to perform detail core analysis of e.g. Material Testing Reactors (MTR) cores at plate and subchannel level.

This work deals with the validation of the high-fidelity coupled Serpent2/Subchanflow, which was modified and extended for the plate/subchannel analysis of MTR-cores, using the data of rod ejection tests performed in the SPERT IV D-12/25 reactor, especially the tests B-34 and B-35 were selected to validate the dynamic capability of Serpent2/Subchanflow. In these unique tests, experimental data e.g. thermal neutron flux, core power evolution during the rod ejection tests, and the plate cladding temperature was measured. It is noted that, due to the lack of detailed information on the initial conditions, the extraction and introduction scenarios of the transient rod for the reactivity insertion required calibrations and assumptions regarding velocity and position.

The comparison of selected parameters predicted by the coupled simulations at plate/subchannel level of the SPERT IV reactor with the measured data at static and transient conditions shows excellent agreement confirming the high accuracy appropriateness of the used code for the analysis of research reactors. The calculated values of thermal neutron flux and core power evolution have a statistical error of $\pm$ 2 sigma. It was also found that the maximum temperature difference between calculated and experimental values is 7 °C and $\sim$ 10 °C for tests B-34 and B-35, respectively. In addition, the coupled code predicts for the first time the temperature of each plate and subchannel considering the local feedbacks between neutronics and thermal-hydraulics allowing the identification of the hottest/coldest plate in the core. The high-fidelity validation tool can provide comparison solutions for current research reactor core analysis methods, such as core analysis with point kinetics or 3D nodal diffusion codes coupled with fuel assembly-level thermal-hydraulics.

1. Introduction

Research reactors have played a key role worldwide as centers of innovation and development in nuclear science and technology for more than six decades. These reactors are used in a variety of fields, including nuclear and particle physics, nuclear medicine, radioisotope production, materials characterization, personnel training, and validation and verification of simulation codes (IAEA, 2014). To date, about 841 research reactors have been built in 70 countries, some of which have been shut down, others are in the repowering process (IAEA, 2022), and some,

* Corresponding author.
E-mail address: victor.sanchez@kit.edu (V. Sánchez-Espinoza).

https://doi.org/10.1016/j.nucengdes.2023.112840
Received 30 August 2023; Received in revised form 14 November 2023; Accepted 12 December 2023
Available online 3 January 2024

such as the Dutch government's PALLAS reactor (Doval et al., 2022) and the Bolivian government's CIDTN reactor (Nogarin, 2016), are in the construction and design phase. Most of these reactors are more than 40 years old and require renewal of their operating license to meet current technical standards and safety requirements (Zuccaro-Labellarte and Fagerholm, 1996; Schaaf et al., 2011; Doval et al., 2022).

To ensure reliable operation of the aging research reactors, it is important to improve their design, performance, and safety. One way to achieve this is through the use of computer codes that model the behavior of these reactors under normal operating conditions and accidental conditions with different level of accuracy and fidelity.

There are a large number of dedicated numerical tools for the analysis transient analysis of research reactors capable of describe the core either with point kinetics methods or using nodal diffusion codes coupled with 1D thermal–hydraulic models (Doval, 1998; Gaheen and Abdelaziz, 2019; Castellanos-Gonzalez et al., 2018). Another line of research was the adaptations of codes used for power reactors (IAEA, 2002; (Adorni et al., 2007) for the analysis of research reactor and its validation is necessary for its application for safety investigations (Soares et al., 2014; Hainoun and Schaffrath, 2001; Bousbia-Salah and Hamidouche, 2005).

A new high-fidelity tool for the detailed plate/subchannel analysis of research reactors was developed recently at Karlsruhe Institute of Technology (KIT) by adapting and modifying the Monte Carlo Serpent 2 and subchannel Subchanflow codes (Almachi et al., 2022a). Initially serpent2/Subchanflow was unrolled, validated and verified for Pressurized Water Reactor (PWR) and Boiling Water Reactor (BWR) (Imke and Sanchez-Espinoza, 2012; Daeubler et al., 2015; Ferraro, 2021; Garcia, 2021).

In this work for the validation of Serpent2/Subchanflow, the experimental data obtained in the SPERT IV reactor and reported by (Crocker and Stephan, 1964) and (Crocker et al., 1963) is used. In (IAEA, 2019), experimental data of several reactors including the one of the reactors SPERT IV D-12/25 are included. Latter provides unique data of neutronic and thermal–hydraulic parameters measured at steady-state and transient conditions. The overall SPERT IV data was extensively used to validate deterministic and stochastic codes (Labit et al., 2021; Motalab et al., 2014). The validation results show that it is necessary to use more sophisticated tools to simulate this reactor due to the high discrepancy between the simulation results and the experimental data (Margulis and Gilad, 2018).

This work is an important step in the validation of the dynamic capability of the high-fidelity code Serpent2/Subchanflow using unique experimental data of the B-34 and B-35 tests performed at the reactor SPERT IV D-12/25 paving the way for the use of this code for safety evaluation of transient of MTR-cores.

The present work is composed of six section. Section 2 presents the main features of the reactor SPERT IV D-12/25, followed by Section 3, which describes the simulation tools and coupling approach. Section 4 introduces the main assumptions for the coupled neutronic and thermal–hydraulic models and simulations. The last two sections, 5 and 6, present and discuss the results of the validation of the Serpent2/Subchanflow, provide the conclusions, and perspectives.

2. The SPERT IV D-12/25 reactor

Fig. 1 shows the Special Power Excursion Reactor (SPERT) built under the U.S. Atomic Energy Commission's reactor safety program. This facility was operated by the Atomic Energy Division of Phillips Petroleum Company to test reactor stability under static and transient conditions (Crocker et al., 1963). In July 1962, the first reactor core used for experimental purposes was designated SPERT IV D-12/25 (Crocker and Stephan, 1964). The diameter of the main tank, which contains the reactor core, is 6.096 m and the depth is 7.62 m. A 0.1064 m flanged nozzle is located in the central part of the bottom of the tank, the cooling fluid flows in an upward way allowing volumetric flow rate of up to 315 L/s through the core. To stabilize the temperature of the coolant surrounding the reactor core, during operation, a cooling system consisting of a 1 MW heat exchanger is used. The drive controls for the control rods (CRs) and the transient rod (TR) are located on the control bridge in the upper part of the containment. A Graham Model 190 MWG variable speed transmission is used to drive the rods. This transmission allows output speeds from 0 to 200 rpm and is controlled by remote electrical control systems (Crocker et al., 1965; Heffner et al., 1962).

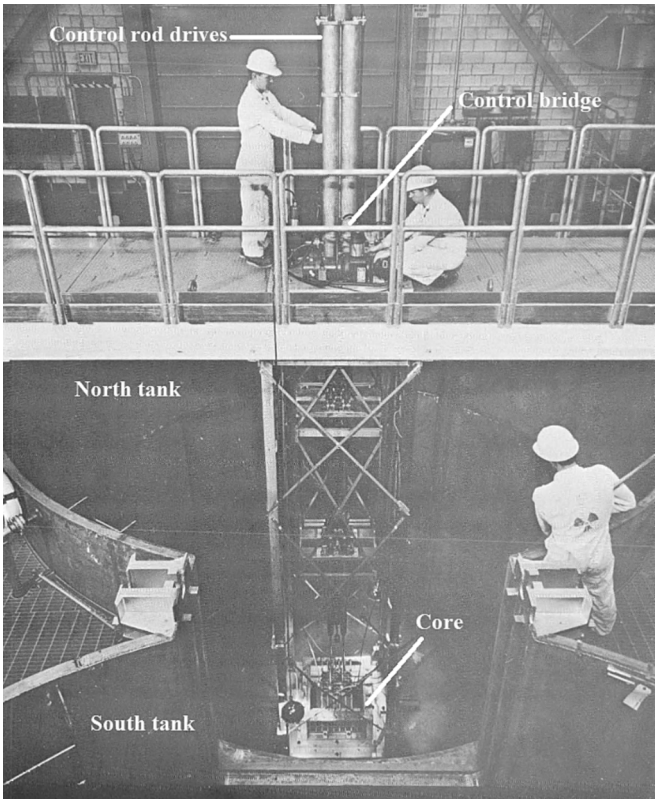

Fig. 1. SPERT reactor facilities, obtained from (Heffner et al., 1962).

2.1. Tests conducted on SPERT IV D-12/25 reactor

The reactor facility SPERT IV D-12/25 was designed to study the kinetic and static behavior of MTR-type reactors. The tests used in this work correspond to the ones obtained in two experimental programs. The first experimental program, called "Nuclear Start-up of the SPERT IV Reactor," collected steady-state thermal neutron flux data and serves to determine the initial criticality condition and reactivity insertion values (Crocker et al., 1963). The second experimental program, called "Reactor Power Excursion Test in the SPERT IV Facility," includes a total of 46 transient tests with reactivity insertion. The main parameters measured in this second phase were the evolution of core power and main fuel plate cladding temperature as a function of time (Crocker and Stephan, 1964).

2.2. Static tests

The experimental results obtained in the first phase of the program SPERT IV D-12/25 have proven useful for the validation of various Monte Carlo codes (Margulis and Gilad, 2018; Motalab et al., 2014). The thermal neutron flux values collected in (Crocker et al., 1963) were measured using cobalt activated wires. Fig. 2 shows a radial section of the reactor core SPERT IV D-12/25, showing the different positions, where the sensors for measuring the thermal neutron flux were placed. Also visible are the control fuel assemblies (CFAs) and the transient fuel

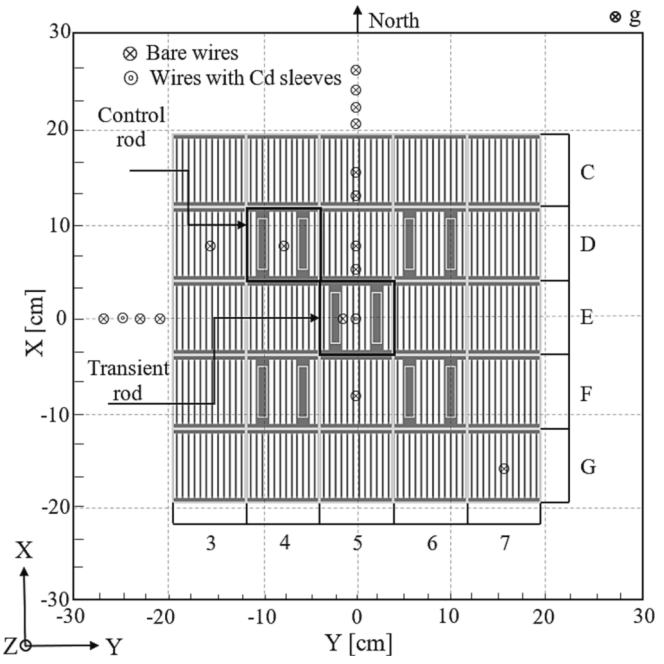

Fig. 2. Two-dimensional representation of a radial cut of the SPERT IV reactor core showing the cobalt wires and the different fuel assemblies.

assembly (TFA). It can be seen that the arrangement of the four CFAs is symmetrical when viewed from the central position where the TFA is located. In this work, the experimental data measured at positions D-4 and E-5 corresponding to the CFA and the TFA are used to validate the Serpent 2 Monte Carlo code.

2.3. Transients tests

A total of 46 transient tests with reactivity insertion were performed in the second phase of the SPERT IV D-12/25 program. The parameters measured in the transient tests include power, energy, temperature and pressure. To validate Serpent2/Subchanflow, the measured values of power and temperature are used. The total core power was obtained from the oscillograph traces recorded in the ion chambers, whose current to power ratios were measured by calorimetric methods. The temperature of the plate cladding was measured using a 0.07 mm thick chromium-aluminum thermocouple (Crocker and Stephan, 1964). It is important to note that the temperature values provided are within 10 % of the values tabulated in the literature, due to errors associated with the digitization of the data (IAEA, 2015). Therefore, a margin of error of ± 10 % for the measured ΔT values is considered in this work.

Among the most common and complex tests to simulate are the so-called B-34 and B-35, which, according to recent recommendations, require more sophisticated computational methods or adjustments of their correlations to reduce the large discrepancy between simulation's results and measured data (Margulis and Gilad, 2018; Labit et al., 2021). In this work, both tests are used to validate the dynamic capabilities of the Serpent2/Subchanflow code.

2.4. Geometric dimensions of SPERT IV D-12/25 reactor

A complete description of the geometric dimensions of the reactor SPERT IV can be found in UK and international units of measurement in (IAEA, 2015) and (Almachi et al., 2022b). This section describes the main dimensions required to create a complete three-dimensional model. Fig. 3(a) shows the base grid that supports the entire core structure. It is made of 60-61T6 aluminum and has 81 internal square cavities that house the different fuel assemblies and irradiation boxes. A radial cut of the reactor core is shown in Fig. 3(b), where the different fuel assemblies can be distinguished. The core consists of 20 standard fuel assemblies, 4 control fuel assemblies and 1 transient fuel assembly. The assembled fuel assemblies are placed in an aluminum mounting box, which is shown in Fig. 3(c).

Fig. 4(a) shows an isometric view of the standard and control fuel assemblies located inside the mounting can. It can be seen that the control and transient fuel assemblies have a rectangular guide in which the control and transient rods move axially to add or remove reactivity to the system.

The control and transient rods are shown in Fig. 4(b); the main difference between the two is the location of the poison material (aluminum alloy containing 7 wt% boron). The poisonous material of the control rod is at the top, while that of the transient rod is at the bottom. Fig. 4(c) shows a top view of the standard and control fuel assemblies. The SFA consists of 12 removable fuel plates, while the C.F.A/T.F.A has a total of six fuel plates distributed among four plates in the center and one plate at each end.

2.5. Operating conditions of the SPERT IV reactor

As mentioned earlier, the tests performed with the SPERT IV reactor were divided into two programs. The first experimental phase records the values measured when the reactor reaches a steady-state. The initial conditions for this series of tests are summarized in Table 1 (Crocker et al., 1963). These parameters are considered in the modeling of the reactor SPERT IV using the Monte Carlo code Serpent 2 stand-alone.

Additionally, experimental data at transient condition are used to validate the dynamic capabilities of Serpent2/Subchanflow. In this second phase of the experimental program, several transient tests were performed. In this work, the experimental data of global power and temperature of the cladding of a critical plate from tests B-34 and B-35 are used (Crocker and Stephan, 1964). The dynamic tests in question analyze the evolution of power and temperature when reactivity is inserted into the reactor core. The initial conditions before recording the transient readings are summarized in Table 2. With respect to the reactivity insertion ramp rate for tests B-34 and B-35 during the transient test, limited information is available. In most analyses, only the maximum reactivity values are used, which are 0.88 $ and 1.05 $, respectively. This limitation implies the need to make certain assumptions in the transient rod movement scenarios, as detailed in Section 5.2.

3. Analysis tools

3.1. Serpent 2 neutronic code

Serpent 2 is a state-of-the-art code developed and distributed by VTT of Finland for particle transport simulation (Leppänen et al., 2015). Serpent 2 simulates the interactions of neutrons with the nuclei of the various materials that make up the reactor and calculates the probability that neutrons will be absorbed, scattered, or escape from the reactor. It is a 3D Monte Carlo continuous energy code that uses the standard ACE Nuclear Data Library (NDL) format to perform static and dynamic calculations (Chadwick et al., 2006). The code is versatile, so it is often used for multi-physics analyses (Leppänen et al., 2012) such as neutronic thermal–hydraulic (Ferraro, 2021; Daeubler et al., 2015) and thermo-mechanical calculations (Garcia, 2021; García et al., 2021). Multi-physics calculations are performed using external interface files called IFC, which can be selected as needed. In this work, the IFC type 22 interface was used (Viitanen and Leppänen, 2012). The multi-physics approach is based on the consideration of parameters that directly affect neutron multiplication, such as the density and temperature of the coolant and fuel. To perform these calculations, Serpent 2 uses rejection sampling techniques in combination with target motion sampling (TMS) (Viitanen and Leppänen, 2014). Serpent 2 is being developed as open source and is written in standard ANSI-C language. It can run on Linux,

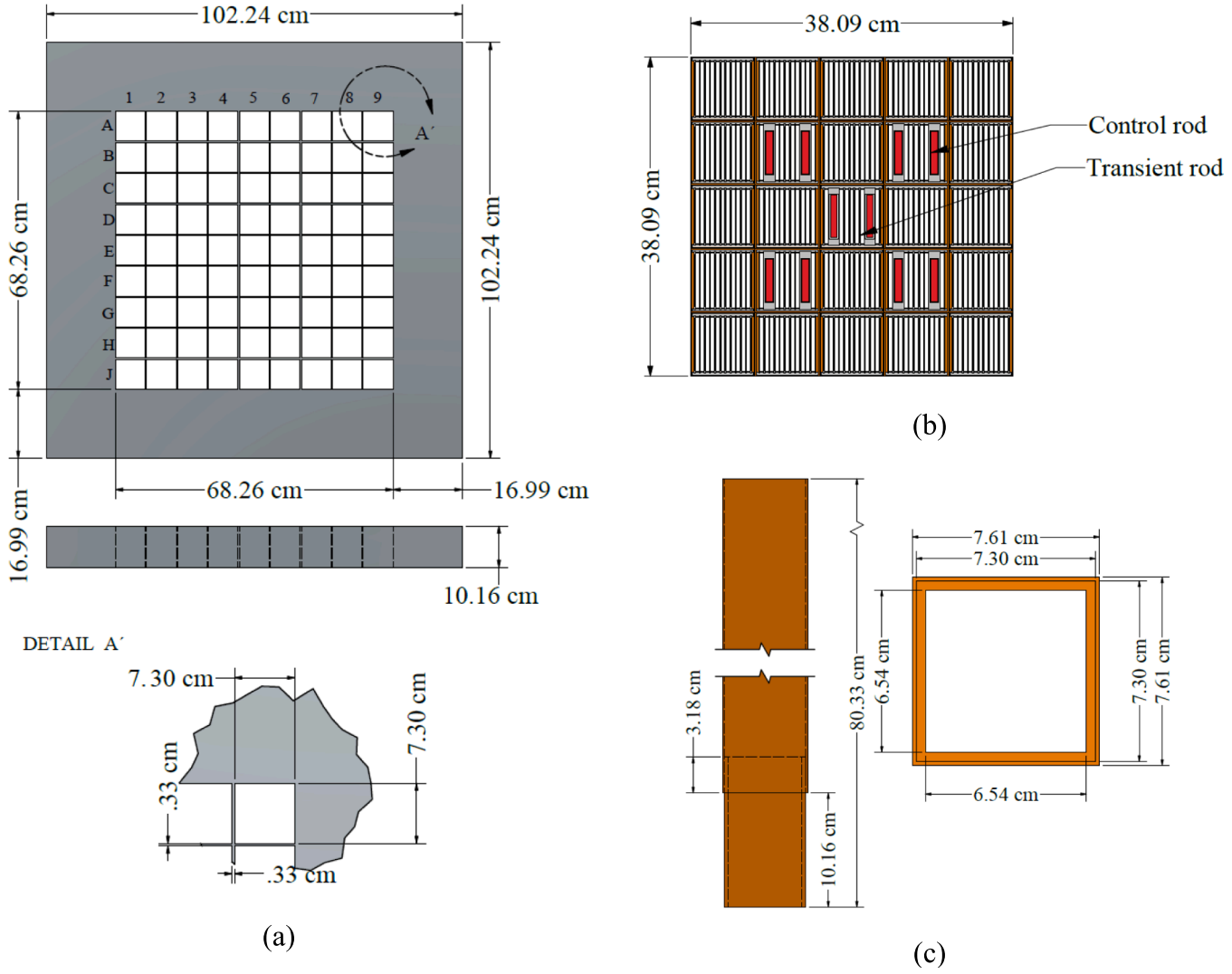

Fig. 3. SPERT IV dimensions in cm of: (a) lower grid; (b) core; (c) assembly can.

so it is highly parallelizable and can take advantage of multi-core processing power when used on supercomputers.

3.2. Subchanflow thermal–hydraulic code

Subchanflow is a thermal–hydraulic subchannel code developed at the Karlsruhe Institute of Technology (KIT) (Imke and Sanchez-Espinoza, 2012). The code allows steady-state and transient calculations for the analysis of Boiling Water Reactors (BWR), Pressurized Water Reactors (PWR) and Water-to-Water Energy Reactors (VVER) reactors. Subchanflow has been extended to model downward and upward coolant flow in MTR research reactors (Almachi et al., 2021). The experimental data used for validation of the latest version of Subchanflow correspond to the RA-6 device and the IEA-R1 reactor (Almachi and Sanchez-Espinoza, 2022c). The code is written in a modular and platform-independent way so that it can be compiled and executed on WINDOWS and LINUX operating systems.

A three-equation flow model is implemented in Subchanflow, which includes mixing equations for the mass, momentum, and energy balances (Basile et al., 1999). In addition, a momentum equation is used for cross-flow between neighboring subchannels. Subchanflow solves the problems for a mixture of two-phase flow using the four conservation equations. A set of empirical correlations and constitutive equations for the wall/liquid heat transfer, pressure drop, etc. are needed to close the system. The mass and energy conservation equations are solved in the subchannel approach for coolant center conditions. Subchanflow is extremely versatile and can be coupled with other codes to perform more accurate reactor analysis. This allows coupled effects to be considered and improves the accuracy in predicting the thermal–hydraulic and neutronic behavior of the reactor.

3.3. Multi-physics coupling approach

The principal-secondary approach is an internal coupling concept developed at the Karlsruhe Institute of Technology for the Serpent 2 and Subchanflow codes. Serpent 2 assumes the role of primary and Subchanflow acts in the role of secondary. This configuration allows for easier compilation and use of the codes. One of the key advantages of this coupling is that it preserves the inherent characteristics of each of the codes and allows the modeling of complex cores such as those found in research reactors. The implementation of principal-secondary approach implies an interdependence between the codes, since the provided calculations are the result of a convergence process of relaxation parameters and thermal–hydraulic fields, such as density and temperature (Ferraro, 2021).

The exchange of thermal–hydraulic fields is done through IFC files. These files contain information about the temperature and density of the coolant and fuel temperature, as well as how this information is stored in

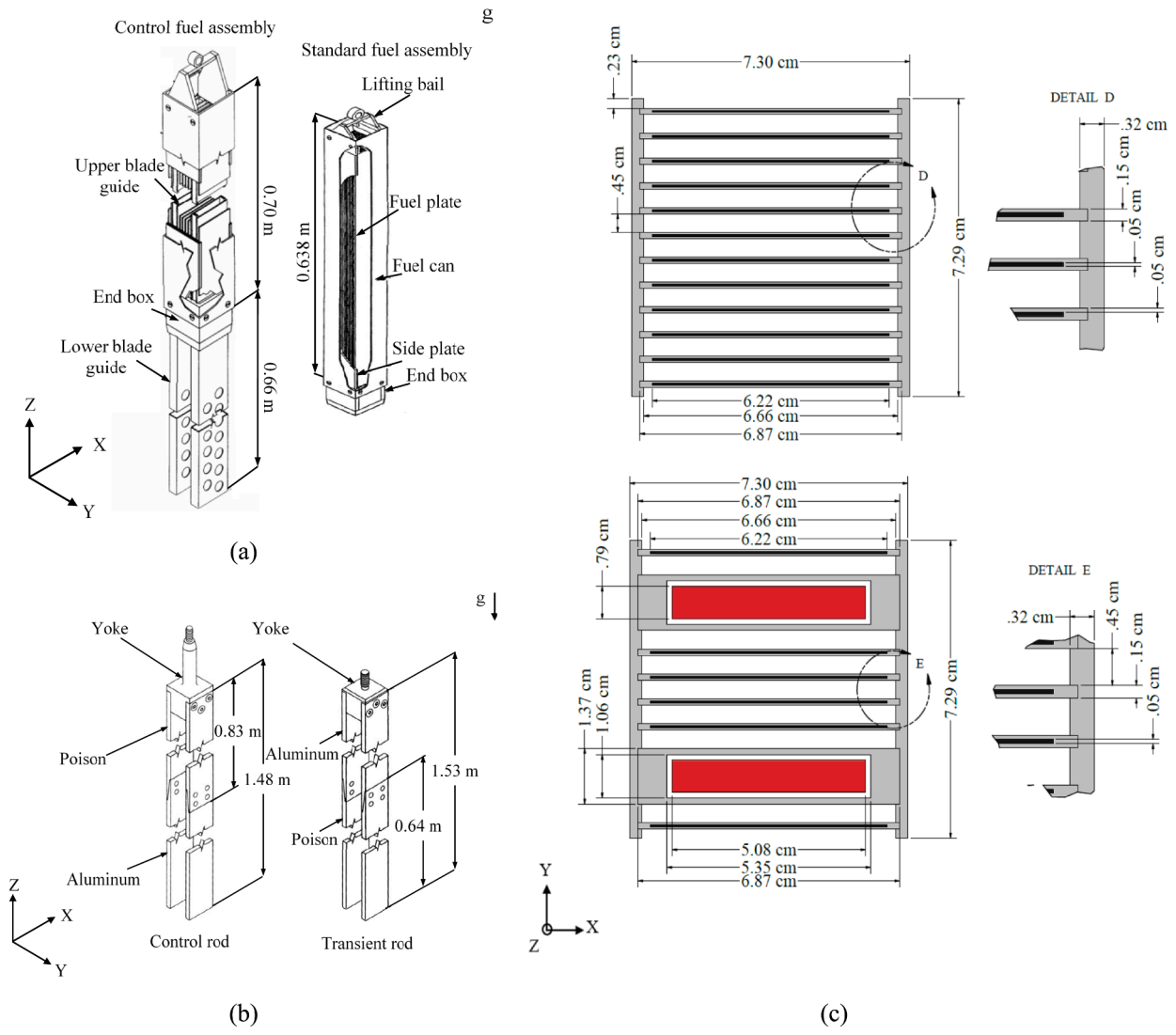

Fig. 4. Details of Assemblies and Control and Transient Rods:(a) isometric view details of SFA and CFA; (b) isometric details of control and transient rods;(c) Radial details of SFA and CFA. Figures (a) and (b) obtained from (IAEA, 2015).

Table 1
Main operating conditions of the reactor SPERT IV D-12/25 for the static calculation.

Parameter	Reference values
Fuel type	UAl alloy Al clad flat plate fuel
Enrichment	HEU 93 % 14.0 g 235 U
Initial temperature	20 [°C]
Coolant, moderator, reflector	Light water
Poison material	Binal (B-Al)
Initial power	1 [W]

Table 2
Global initial conditions for SPERT IV D-12/25 for the transient calculations.

Parameter	Test B-34	Test B-35
Inlet pressure [Pa]	140,000	140,000
Reactor power [W]	62,548	68,495
Temperature inlet [°C]	21.9	22.0
Inlet volumetric flow rate [L/s]	315.45	315.45

a spatial grid. The grids containing this information are superimposed on the geometric model created in Serpent 2 and Subchanflow, transferring the information from cell to cell, which allows the creation of complex

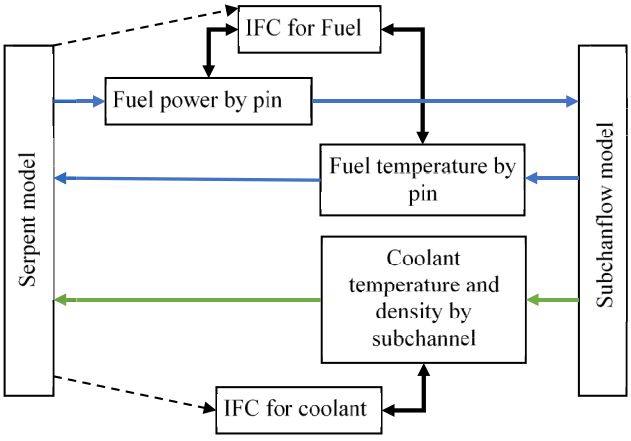

Fig. 5. Concept of thermal–hydraulic field exchange in a coupled model, adapted from (Ferraro, 2021).

lattice structures such as those present in PWR, VVER and MTR reactors. The concept of field exchange within the coupled code is illustrated in Fig. 5, where two IFC files are shown, one for the fuel and one for the coolant. The model created in Serpent 2 provides the power values generated by nuclear fission to the Subchanflow thermal–hydraulic code. The power provided by Serpent 2 is an average value per fuel plate that is converted and transmitted to Subchanflow as needed. The thermal–hydraulic code then performs fuel, cladding, and coolant temperature calculations, and when convergence conditions are reached, the average cells values of fuel temperature, coolant temperature, and coolant density are transferred to Serpent 2. All fields are stored in RAM, which allows fast and efficient data exchange.

3.4. Simulation of transients with Serpent2/Subchanflow

The neutron transport equation with time dependence is essential for understanding the behavior of a reactor. This type of problem usually deals with the occurrence of prompt and delayed neutrons. The occurrence of both groups of neutrons in Serpent2/Subchanflow will be treated taking into account the considerations of (Sjenitzer, 2013). Prompt neutrons are treated as instantaneous because of the short time in which they are released (10E-14 s), while delayed neutrons are evaluated by tracking the precursor population that produces them. To address the transient problems with Serpent2/Subchanflow the two-step approach must be followed. In the first step, two sources are created and stored; one of the sources considers neutrons traveling with a certain position, direction, and energy, commonly known as live neutrons, and the other source stores the precursor population. Both sources are stored in external files and must be calculated from a critical state of the core. In the second step, the external files obtained in step 1 are used for the transient calculation, which is analogous to the fixed source method as a function of time (Ferraro, 2021; Sjenitzer, 2013; Sjenitzer and Hoogenboom, 2011; Valtavirta et al., 2016).

4. SPERT models and setup of coupled simulations

4.1. Serpent 2 model

Following the geometrical specifications of Section 2.1.3, the detailed three-dimensional representation of all components of the D-12/25 SPERT IV reactor is performed using Serpent 2. The developed model is used for validation of the static thermal neutron flux calculations and elaboration of the integral control rod worth profile. For the steady-state calculations, the following aspects were considered:

- The nuclear data library used was ENDFB-VIII.0.
- To obtain the thermal neutron flux values, counters were used at positions D-4 and E-5 (see Fig. 2). The mesh of counters is formed by a square of 0.10 cm side in the XY plane extruded 77.15 cm in the Z direction, dividing into 60 equidistant axial cells.
- Each calculation is performed with 200 inactive cycles followed by 1000 active cycles, with a neutron population of 1E6 per generation.
- The energy cutoff for thermal flux was set to 0.5 eV.
- Vacuum boundary conditions are used for the radial and axial core boundaries

4.2. Subchanflow model

To create a representative model of the SPERT IV D-12/25 reactor with the Subchanflow code, a radial map has been created representing the location of each plate and channel. This representation can be seen in Fig. 6. The following assumptions are made as follow:

- The central plate model is used for thermal–hydraulic data transfer.
- The lateral number of nodes for heat conduction is divided into 3 nodes for the fuel and two nodes for the cladding.

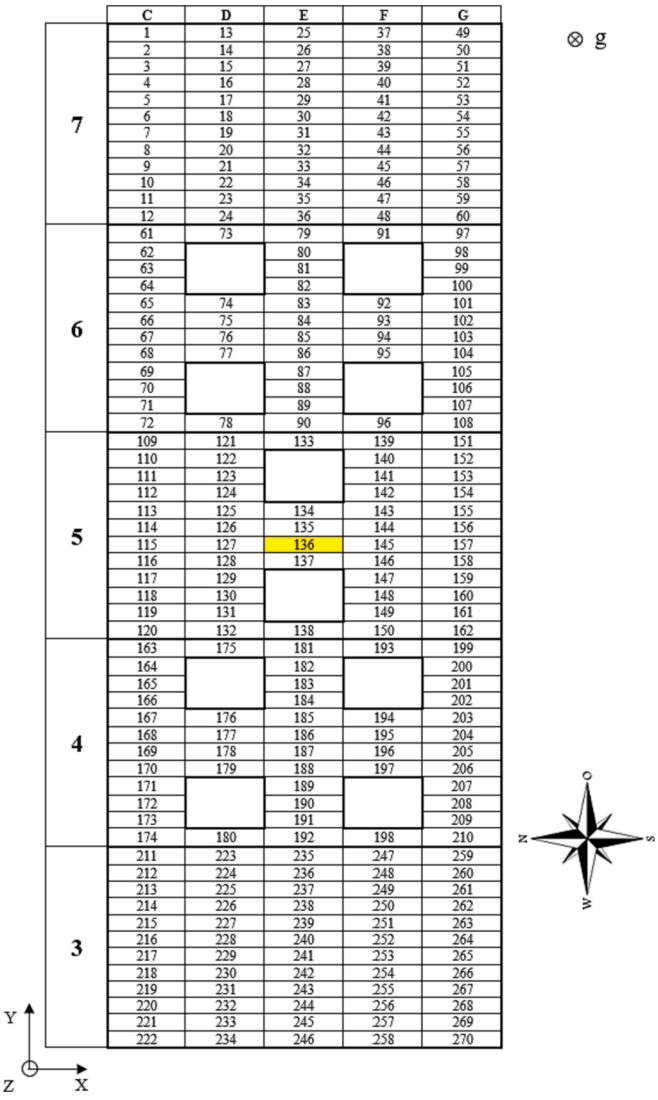

Fig. 6. Top view for the identification of plates and cooling channels, for remapping between Serpent 2 and Subchanflow, SPERT-IV reactor.

- The axial discretization for the IFC information transfer is 20 cells for both the fuel plate and the coolant channel.

As in the case of the IEA-R1 reactor, it has been observed in several studies that the use of standard heat transfer correlations, such as Dittus-Boelter or similar, leads to high values for the plate cladding temperature (Margulis and Gilad, 2018; IAEA, 2019; Labit et al., 2021). To improve the simulation results other correlations more appropriate for MTR-fuel assemblies are selected based on the validation of Subchanflow (Almachi and Sanchez-Espinoza, 2022c). Consequently, the use of the Y-Sudo correlation was selected for this work (Sudo et al., 1990). In addition, the friction factors for laminar and turbulent flows shown in (Li and Zhang, 2010) and (Rohsenow et al., 1998) are selected.

4.3. Setup of the coupled Serpent2/Subchanflow simulation

A Serpent2/Subchanflow simulation is performed with the models described above for a detailed plate/subchannel level three-dimensional analysis of the SPERT IV D-12/25 transient tests. Due to the high complexity of the reactor core, additional files are used for axial and radial re-assignment of nodes in both cases. The analyses performed in two steps: a static and dynamic calculations.

Step1: static calculations:

- The axial discretization for the information transfer (IFC type 22) is 20 cells for both the fuel plate and the coolant channel; and
- the calculations are performed with 200 inactive cycles followed by 1000 active cycles, with a neutron amount of 1E6 per generation.

Step2: dynamic calculations:

- For tests B-34 and B-35, the total number of particles is 4E6, divided into 200 batches,
- The axial discretization for the information transfer (IFC type 22) is 20 cells for both the fuel plate and the coolant channel.
- The insertion of reactivity to the system is performed by the combined movement of extraction and insertion of the transient rod (see Fig. 13).
- The typical convergence values for the thermal–hydraulic feedbacks used in this work correspond to those proposed by (Ferraro, 2021; Ferraro et al., 2019) ($\in^{\sim t}_{T_{fuel}} \leqslant 5\ [^{\circ}C]$, $\in^{\sim t}_{T_{cool}} \leqslant 1\ [^{\circ}C]$ and $\in^{\sim t}_{\rho_{cool}} \leqslant 0.01\ [g/cm^3]$). Also, the ω -factor for the relaxation of the thermal–hydraulic parameters for steady-state and transient calculations is equal to 0.5 and 0.0, respectively.

5. Discussion of results

5.1. Validation of Serpent 2 using steady-state experimental data

The experimental parameters used for the validation of Serpent 2 are divided into two groups: the control rod worth as a function of the axial position and the axial distribution of the normalized neutron flux at positions D-4 and E-5. Fig. 7 shows the curve of the experimental reactivity values together with the values calculated by Serpent2/Subchanflow. The reactivity values increase as the control rods are removed from the reactor core, increasing in neutron flux. Six axial positions were selected for comparison, each one simulated according to the specifications given in Section 4.1. The statistical error bars of the calculated values correspond to ± 2 sigma and include all experimental values, indicating good agreement.

Once the reactivity curve is obtained, the axial position of the control rods for a criticality condition is calculated. The neutronic parameters obtained under such conditions are listed in Table 3. Fig. 8 shows the position of the control rods and the transient rod. In this set of calculations, the poisonous section of the transient rod is completely outside the core, unlike the control rods. The poisonous section of the control rods is at 51.46 cm, measured from the lowest part of the reactor.

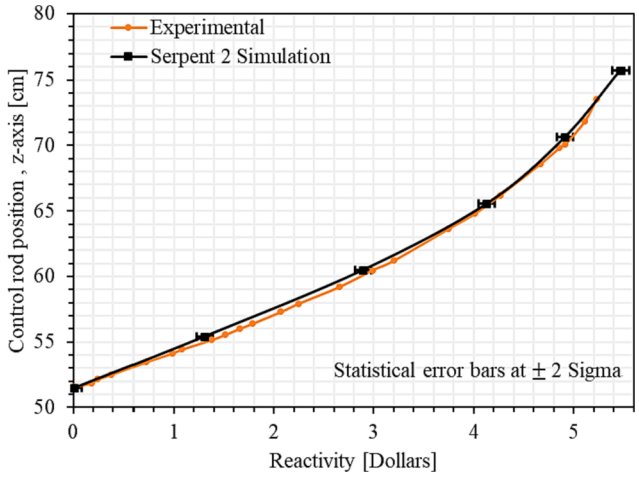

Fig. 7. Experimental and calculated control rod worth curve as a function of different positions of the reactor control rod SPERT IV D-12/25; all control rods are removed at the same time.

Table 3
Comparison between experimental and predicted values for the main neutron parameters.

Item	$\Lambda/\beta_{eff}\,[ms]$	k_{eff}	Critical position with T.R. fully out [cm]	Excess reactivity [$]
Experiment	8.1	~ 1	51.46	5.27
Serpent 2	8.3 ± 0.02	1.00007 ± 0.00014	51.46	5.27 ± 0.04

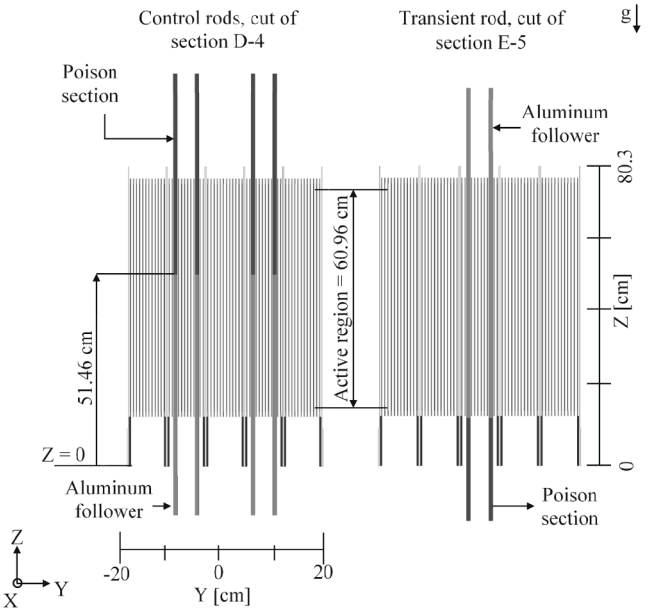

Fig. 8. Representation of the SPERT IV reactor using Serpent 2 together with axial sections for the control (section D-4) and transient (section E-4) rods.

Figs. 9 and 10 show the normalized values of thermal neutron flux, both measured and calculated with Serpent 2. In both figures, the peak values of neutron flux are observed at a height of about 40 cm, measured from the bottom of the reactor core. Fig. 9 shows that the neutron flux in D-4 is lower in the upper part of the reactor core, which is due to the presence of the poisonous section of the control rods that limits neutron production. On the other hand, when comparing the profiles in E-5 (Fig. 10), it is observed that the neutron flux is higher than in D-4, which is because in E-5 the poisonous material of the transient rod is located outside the reactor core and does not directly affect the neutron population.

Comparing the values calculated by Serpent 2 with the experimental values, a good agreement between them is observed. Moreover, statistical error bars of ± 2 sigma have been considered. It can be observed that the maximum error bars occur at the peaks of the neutron flux distribution. These results confirm the validity of the established model and that the results are consistent with those presented by (Margulis and Gilad, 2018) and (Motalab et al., 2014).

5.2. Validation of Serpent2/Subchanflow using transient experimental data

5.2.1. Start-up of the SPERT IV reactor

Details about the start-up of the transient experiments are documented in (Crocker and Stephan, 1964) and (Spano and Miller, 1962). A similar procedure is followed to determine the initial starting positions of the control rods and the transient rod in the simulations:

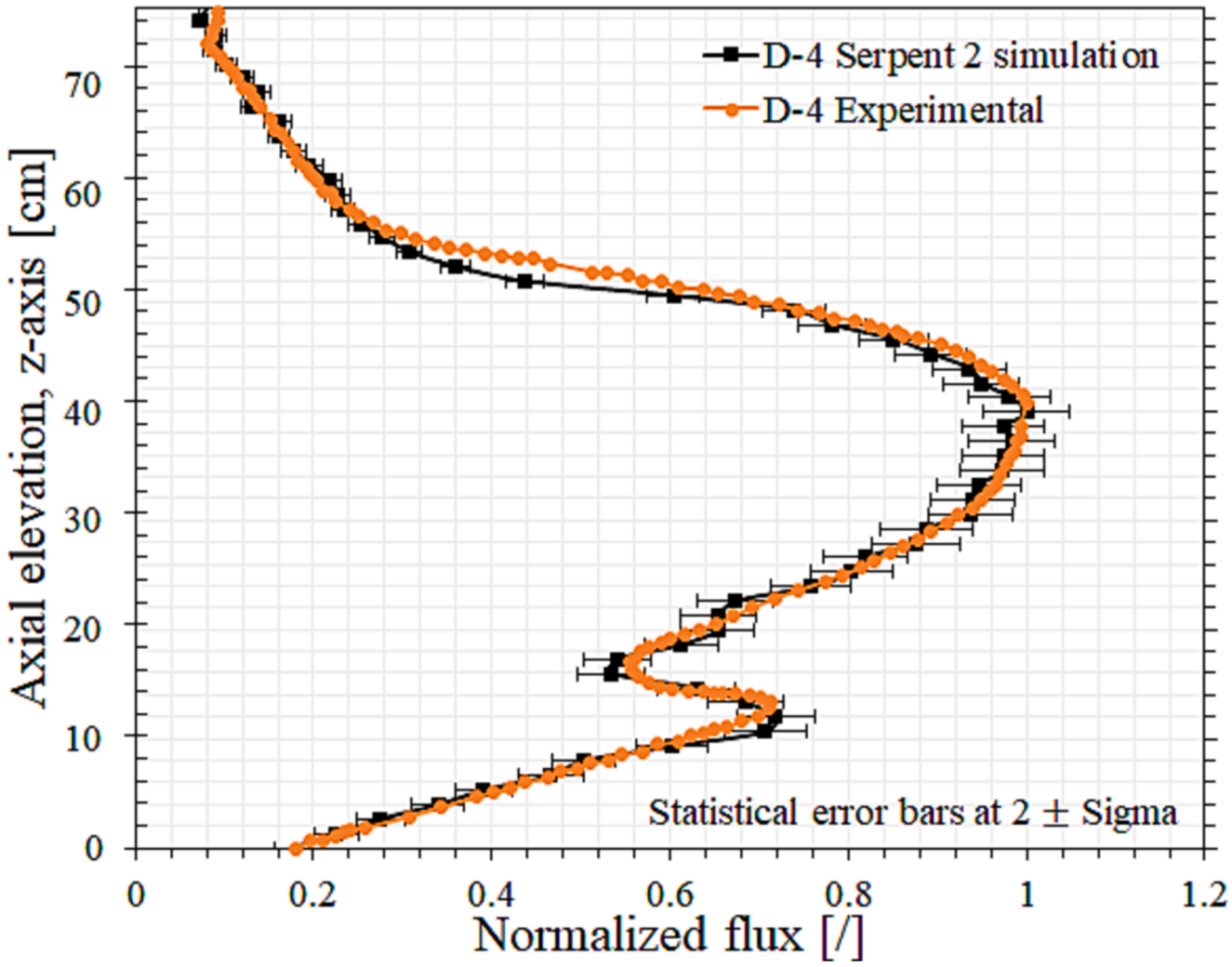

Fig. 9. Comparison of thermal neutron flux detector at location D-4.

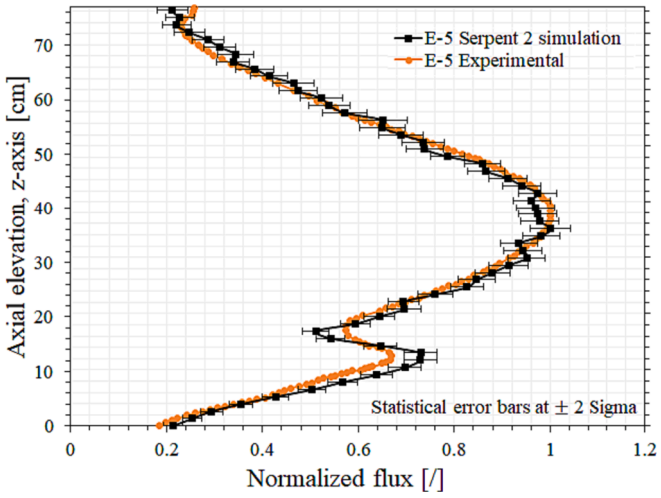

Fig. 10. Comparison of thermal neutron flux detector at location E-5.

1. Criticality condition: In this case, the model validated in Section 5.1 is used, where the positions of the control and transient rods are known (see Fig. 8).
2. Adding reactivity to the system: Within the framework of the transient tests carried out in the SPERT IV D-12/25 reactor, a reactivity variation was recorded that ranged from 0.88 $ to 2.14 $. Following the calibration guidelines outlined in (Spano and Miller, 1962), it was established that the reactivity generated by the transient rod should overestimate the value obtained in the test, which, in this context, was 2.14 $. Given the limitation of detailed information on this procedure in the present work, for the overestimation it was decided to add a conservative value of 0.5 $ to the maximum value observed in the test. As a result of this adjustment, a new rectified value for reactivity was calculated, which amounts to 2.64 $.
3. Control rods position: Using the reactivity value of 2.64 $ and the control-rod-worth- curves shown in Fig. 7, the position of the control rods is calculated. The control rods are pulled out until the calculated position is reached.
4. Transient rod position: The absorber material section of the transient rod is inserted into the reactor core until a criticality value is again reached, i.e., a value of 2.64 $ is extracted from the system. At this point, the positions of the control rods and the transient rod are recorded.

The sequence of steps has been addressed for the initial conditions given in Table 1 and the assumptions described in Section 4.3. Fig. 11 shows the Serpent2/Subchanflow model created to simulate the reactor SPERT IV D-12/25. It shows the axial sections to illustrate the position of the control rods and the transient rod. In slice D-4, it can be seen that the

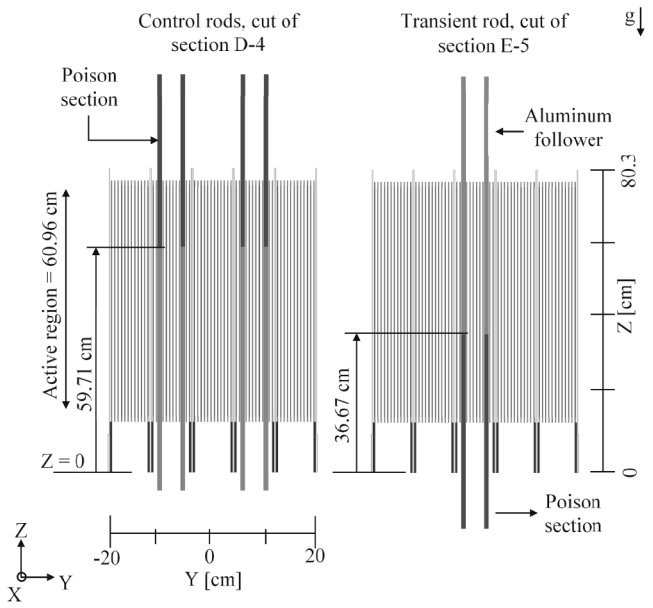

Fig. 11. Representation of the SPERT IV reactor using Serpent2/Subchanflow together with axial sections for the control (section D-4) and transient (section E-4) rods.

position of the control rods is 59.71 cm measured from the bottom. It has been determined using the rod-worth control curves (Fig. 7); in slice E-5, the poisonous section of the transient rod can be seen at a distance of 36.67 cm measured from the bottom. Fig. 12 shows the value curve of the transient rod created using seven axial positions. The distances shown in this section correspond to a criticality condition relevant to the transient test. This configuration is used for calculating and storing of the external sources of live neutrons and precursors required for the dynamic calculations (see Section 3.4).

5.2.2. *Transient rod movements scenarios for reactivity insertion*

The scenarios for transient rod motion during dynamic tests in the SPERT IV D-12/25 reactor is not adequately documented. Also, since this is the first time this reactor has been modeled with high-fidelity codes, there is no clear proposal on how to address this problem. To solve this situation, it is proposed to use the method already used in the reactor SPERT III, where the problem of reactivity insertion was solved by extracting the transient rod at constant velocity and then, in order to reduce reactivity, the transient rod was re-introduced at constant speed at certain time intervals (Ferraro et al., 2020; Ferraro, 2021).

For tests B-34 and B-35, the determination of the extraction and introduction velocities of the transient rod is the result of a previous calibration process. I.e., in the case of test B-35 submitted by (Almachi and Sanchez-Espinoza, 2023), the power curve (see Fig. 16) shows two noticeable increases: a sudden one, occurring up to t = 1.54 s, and a more gradual one, extending up to t = 2.74 s. The first increase in power is associated with the rapid removal of the control rod, while the second is due to the residual effects of the initial disturbance that gradually evens to equilibrium. From t = 2.74 s, the slope of increase is observed to be smaller than previously observed, suggesting a reduction in fission reactions, associated with the introduction of the poisonous section of the transient rod. To simulate this second behavior, the transient rod is introduced on two occasions. This process is summarized in Fig. 13 for tests B-34 and B-35.

Regarding the experimental data used to validate the Serpent2/Subchanflow code, the power and temperature values were measured at time intervals of 9 s and 4 s for tests B-34 and B-35, respectively. For the transient simulation, the time intervals for both cases are summarized in Table 4, which are divided into 100 bins, thus obtaining time steps of 0.09 s for B-34 and 0.04 s for B-35.

5.2.3. *Comparison of global reactor parameters for the test B-34*

Fig. 14 shows the evolution of the average experimental power of the reactor core SPERT IV D-12/25 together with the power values calculated by Serpent2/Subchanflow and the ramp of reactivity insertion into the system. It can be observed that the reactivity added to the system increases rapidly when the poisonous section of the transient rod (see Fig. 11) is removed from the core, reaching a maximum value of 0.746 ± 0.04 $ at a time of 1.96 s. Subsequently, the reactivity begins to decrease and tends to stabilize. This increase in reactivity results in an increase in power, as shown in Fig. 14. The values calculated by Serpent2/Subchanflow, which contain a statistical error band of ± 2 sigma, show a good approximation to the experimental values. Large variations in the calculated values from the measured data are not observed, confirming a good prediction capability of the high-fidelity coupled code the analysis of short transient considering local feedbacks between neutronic and thermal–hydraulic phenomena of research reactor cores.

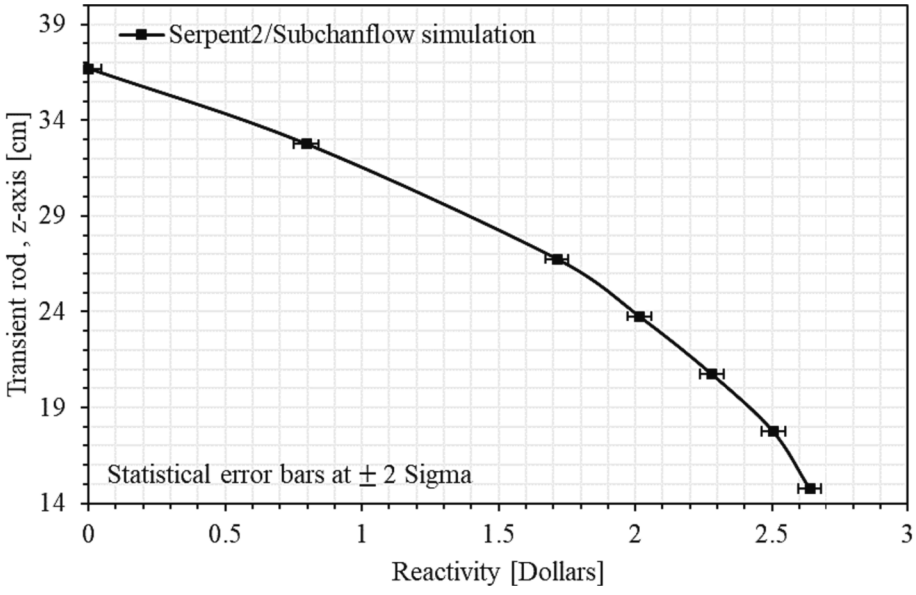

Fig. 12. Calculated reactivity curve as a function of different positions of the reactor transient rod SPERT IV D-12/25.

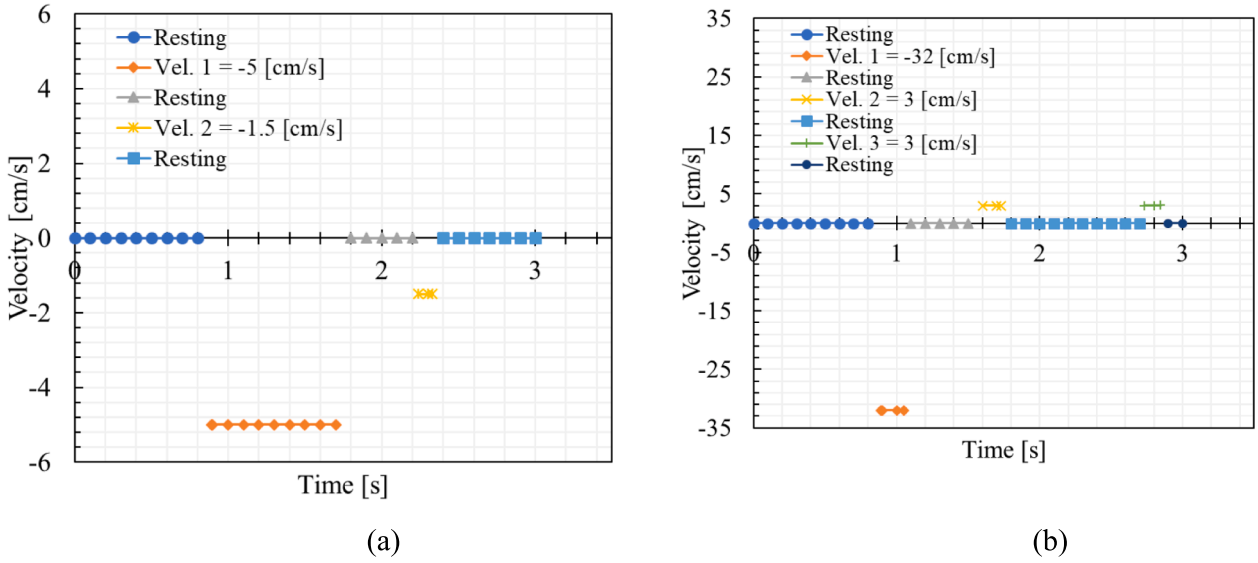

Fig. 13. Proposed transient rod movement scenarios for: (a) the reactivity insertion of 0.88 $ for the B-34; (b) reactivity insertion of 1.05 $ for the B-35.

Table 4
Experimental time and simulation Δ time for cases B-34 and B-35.

I.D.	Experimental time [s]	Simulation Δt [s]	Bins	Step-time [s]
B-34	0.89 – 9.89	9 [s]	100	0.09
B-35	0.89 – 4.89	4 [s]	100	0.04

Fig. 15 shows the evolution trend of the average temperature of the fuel and coolant in the core of the SPERT IV D-12/25 reactor predicted by the coupled code. It is observed that the temperature values reached by the fuel are higher than those of the coolant (82.40 °C vs. 32.7 °C in 9.89 s). In addition, more pronounced fluctuations are observed in the temperature profile of the fuel compared to the coolant. In both cases, the temperature values calculated by Serpent2/Subchanflow do not exceed the boiling limits of the coolant or the melting point of the fuel, ensuring safety margins. The more noticeable fluctuations, observable after 4 s, in the fuel temperature curve are the result of the inherent stochastic nature of the simulation method. The unpredictable nature of neutron interactions and other probabilistic processes occurring within Serpent 2 can cause variations in the simulated results in Subchanflow (see Fig. 5). Although increasing the number of simulation particles or variance reduction techniques could mitigate fluctuations, their implementation could significantly increase computational costs in the former case and in the latter, it appears that the variance reduction technique has limitations with examples where transient rods or control rods are removed (Ferraro, 2021).

5.2.4. *Comparison of global reactor parameters for the test B-35*

As in case B-34, Fig. 16 shows the experimental power values measured in the SPERT IV D-12/25 reactor together with the power and reactivity values calculated by Serpent2/Subchanflow. It can be seen

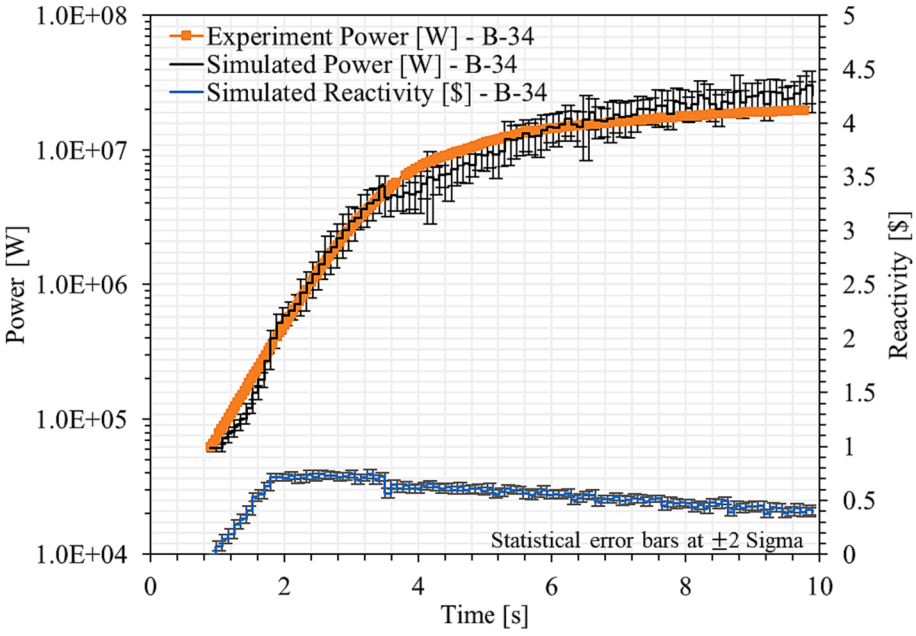

Fig. 14. Evolution of total reactor power and total system reactivity of the reactor SPERT IV, only power values are compared with experimental measurements reported for B-34.

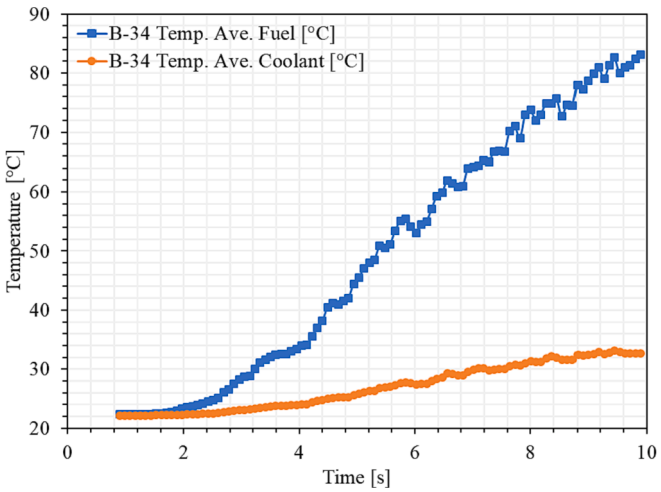

Fig. 15. Evolution of core averaged fuel and coolant temperature calculated by Serpent2/Subchanflow for the SPERT IV reactor tests B-34, no experimental results are provided for comparison.

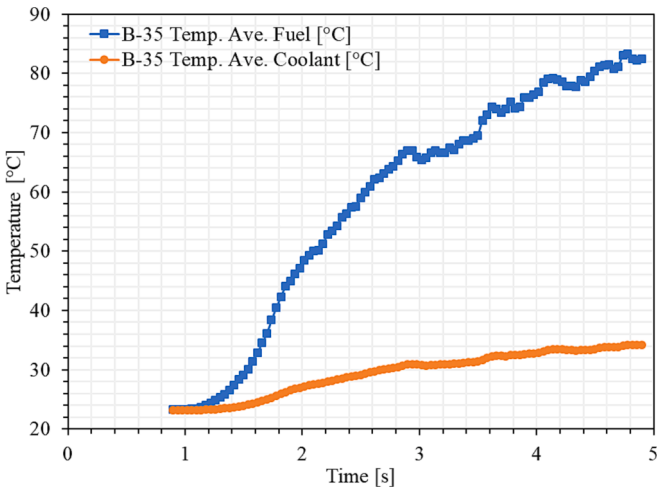

Fig. 17. Evolution of core averaged fuel and coolant temperature calculated by Serpent2/Subchanflow for the SPERT IV reactor tests B-35, no experimental results are provided for comparison.

that the experimental power values increase in at least two different time intervals. In the first-time interval, the power experienced increases rapidly and reaches a value of 8.65 MW at t = 1.56 s. Subsequently, the power continues to increase but at a lower intensity until it reaches 21 MW at t = 4.89 s.

Regarding the calculated values, it can be seen that the reactivity increases rapidly when the poisonous section of the transient rod leaves the core according to the scenarios proposed in Fig. 13, which in turn causes an increase in power. Then, when the rods are reintroduced, the fission energy production decreases, but there is no immediate drop in power. The scenarios for the movement of the control rods are matched to the reactivity curve that controls the calculated power profile. The reactivity curve, located at the bottom of Fig. 16, shows an increase to a maximum of 0.95 ± 0.04 $ at t = 1.13 s and then begins to drop to a value of 0.55 ± 0.044 $ at t = 4.89 s. The reactivity curve is then used to calculate the power profile. Comparing two sets of values shows that 95 % of the experimental values are within the ± 2 sigma error bar, confirming the good agreement between the two data sets.

Fig. 17 shows the evolution of the core average temperatures for the fuel and coolant calculated by Serpent2/Subchanflow, up to a time of 4.89 s. It can be seen that the coolant and fuel temperatures reach their maximum values of 34.0 °C and 84.0 °C, respectively. Similar to Fig. 15, the fluctuations observed in the fuel temperature profile (starting at 2.9 s) are inherent to the Monte Carlo approach i.e. due to the statistical uncertainties. It should be noted that, in this case, experimental data are not available for comparison either; however, these results are valuable for calculations performed with lower level solvers, such as deterministic methods. The absence of an uncertainty estimate at this stage is an aspect to consider.

5.2.5. *Comparison of local reactor parameters for the test B-34*

A major advantage of the Serpent2/Subchanflow code is its ability to calculate parameters at the local level, i.e., at the plate/subchannel level, considering the feedback between neutronics and thermal-hydraulics. Fig. 18 shows the radial power distribution for each of the plates of the SPERT IV D-12/25 test B-34 for a time of 9.89 s. In this figure, the plates with maximum and minimum power can be identified which according to Fig. 6, can be named # 182 (with 118030 W) and # 5 (with 66995 W), respectively. The power concentration is mainly located in and around the center of the core. The plates near the water channels, where the control rods and the transient rod moves, have higher power due to the increased moderator effect of the water present in these channels.

The three-dimensional representation of the cladding temperature distribution, shown in Fig. 19, is of great interest. As with power, the maximum temperature values are concentrated in the center of the core

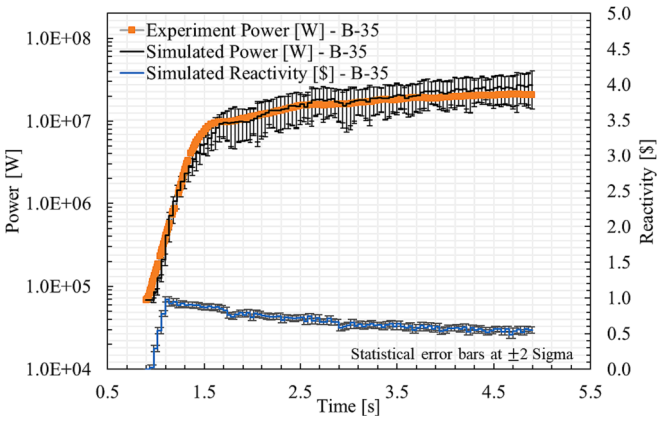

Fig. 16. Evolution of total reactor power and total system reactivity of the reactor SPERT IV, only power values are compared with experimental measurements reported for B-35.

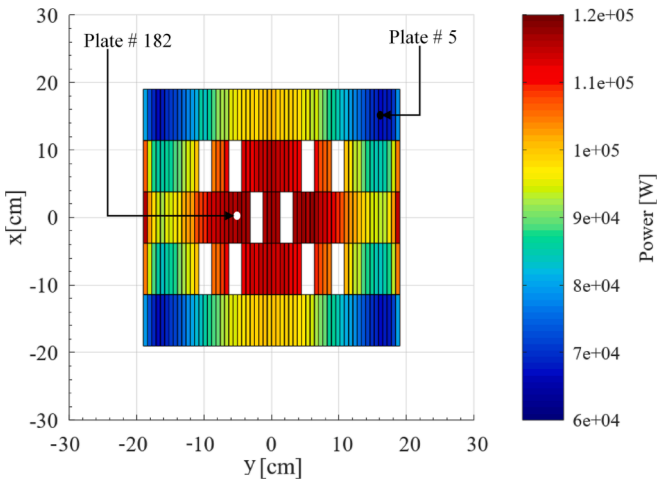

Fig. 18. Radial power distribution for the SPERT IV reactor calculated by Serpent2/Subchanflow, test B-34 at a discrete time of t = 9.89 s after reactivity insertion.

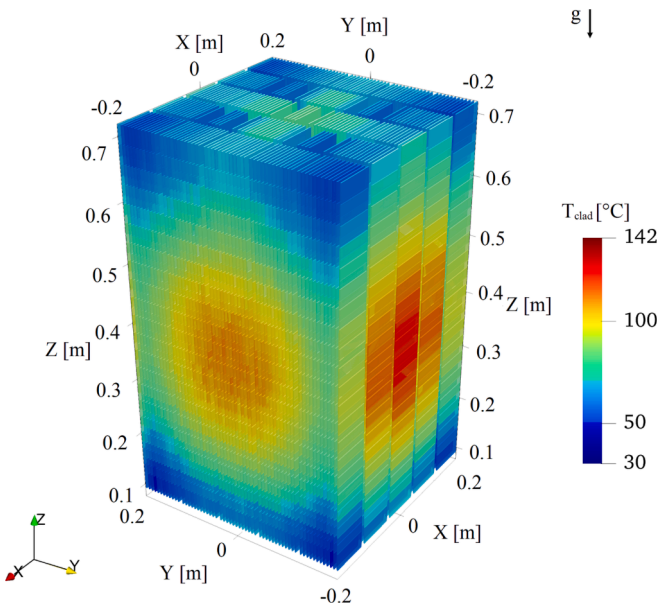

Fig. 19. 3D cladding temperature distribution of reactor SPERT IV D-12/25 test B-34, predicted using Serpent2/Subchanflow at t = 9.89 s.

due to the high neutron flux. The temperature profiles for plate/channel #182 and #5 are shown in Fig. 20. The maximum temperature values for plate # 182 are located at a distance of 43.71 cm from the lowest part (see Fig. 11) and correspond to 139.46 °C for the fuel and 131.33 °C for the cladding. Also, for the lowest power plate, # 5, the highest temperature values are measured at a height of 43.71 cm with 87.09 °C for the fuel and 83.43 °C for the cladding. For the coolant temperature profiles, the maximum values are observed at the core outlet with values of 45.62 °C for channel # 182 and 38.47 °C for channel # 5, respectively. It is important to note that this data set does not show large discrepancies or significant fluctuations, demonstrating the consistency of the developed models.

Fig. 21 shows the experimental temperature values of the cladding of plate # 136 compared to the values calculated by Serpent2/Subchanflow. The experimental temperature corresponds to those measured up to a time t = 9.89 s with a thermocouple at position x, y, z (0, −0.03, 35.08) cm. The uncertainty bar considered for the experimental data corresponds to 10 %, as stated in (IAEA, 2015). It can be observed that the calculated values over- and under-predict the temperature values; but 98 % of the calculated values are within the considered uncertainty bar. Large fluctuations are not observed during the temperature evolution, and the maximum difference between the predicted and experimental values is about 7 °C at time t = 9.89 s. This excellent agreement between the experimental data and the calculations performed with Serpent2/Subchanflow demonstrates the high accuracy of the applied numerical tools to perform detailed plate/subchannel level calculations of research reactors cores under transient conditions.

5.2.6. *Comparison of local reactor parameters for the test B-35*

Similar to test study B-34, the results for power and temperature for test B-35 are presented and discussed hereafter. Fig. 22 shows the average radial distribution of power for each of the plates. It can be seen that the high-power distribution is mainly in and around the core center. In addition, the plates near the empty spaces through which the control rods and the transient rod transit also get more power due to the presence of the coolant, which acts as a moderator facilitating the generation of fission energy. In test B-35, the plates with the highest and lowest power are located on the left side of the core, at time t = 4.89 s. These plates correspond to plate # 246 with a power of 116240 W and plate # 219 with a power of 65304 W, respectively.

The three-dimensional representation of the temperature distribution for the cladding of each of the plates is shown in Fig. 23, where it can be seen that the plates with the highest temperature values are located in and surrounding the center of the core, which is consistent with the power distribution shown in Fig. 22. The temperature profiles for plates/channels # 246 and # 219 are shown in Fig. 24, where the axial temperature distribution for the fuel, cladding and coolant can be seen. For plate # 246, the temperature peaks of the fuel and the cladding are located at a distance of 43.71 cm from the bottom of the reactor and correspond to 122.74 °C and 115.85 °C, respectively. In addition, it is found that for the plate with the lowest power, the temperature peaks for the fuel and the cladding are located at a height of 46.76 cm, measured from the bottom of the reactor, with values of 84.68 °C and 80.68 °C, respectively. Regarding the coolant temperature, of the channels # 246 and # 219, the maximum values are found at the core outlet and correspond to 48.87 °C and 38.45 °C, respectively. Fluctuating values with large discrepancies with each other cannot be observed. Since no experimental data are available for these parameters, the values predicted by Serpent2/Subchanflow can be considered as comparison values for low-order solvers, such as diffusion codes or point kinetics.

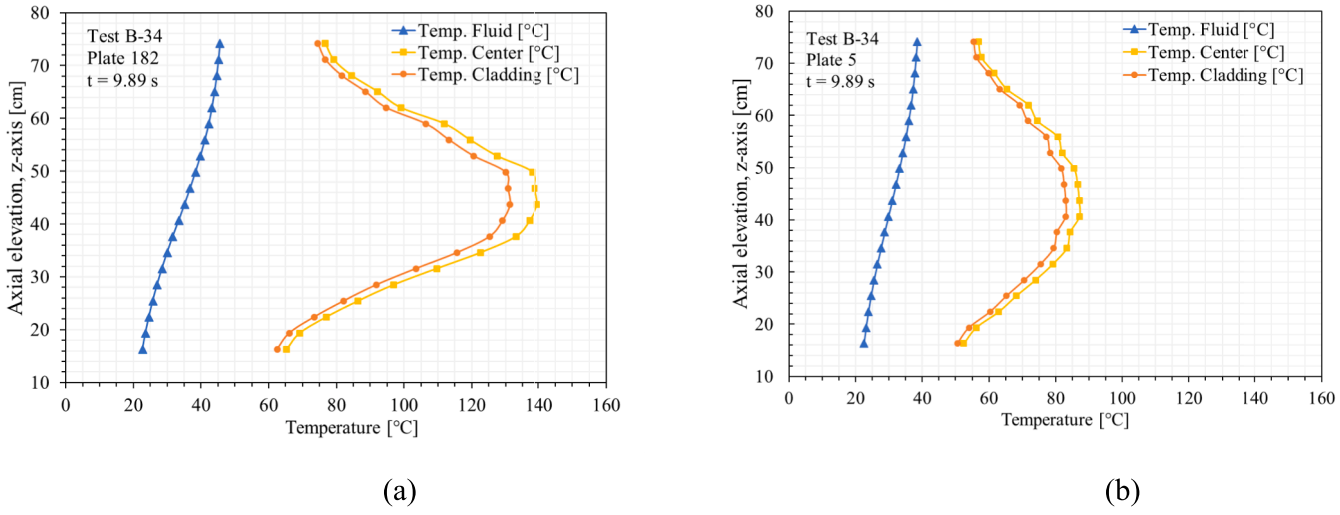

Fig. 20. Test B-34, axial temperature distribution for coolant, cladding and fuel for: (a) maximum power plate # 182; (b) minimum power plate # 5 at t = 9.89 s after reactivity insertion.

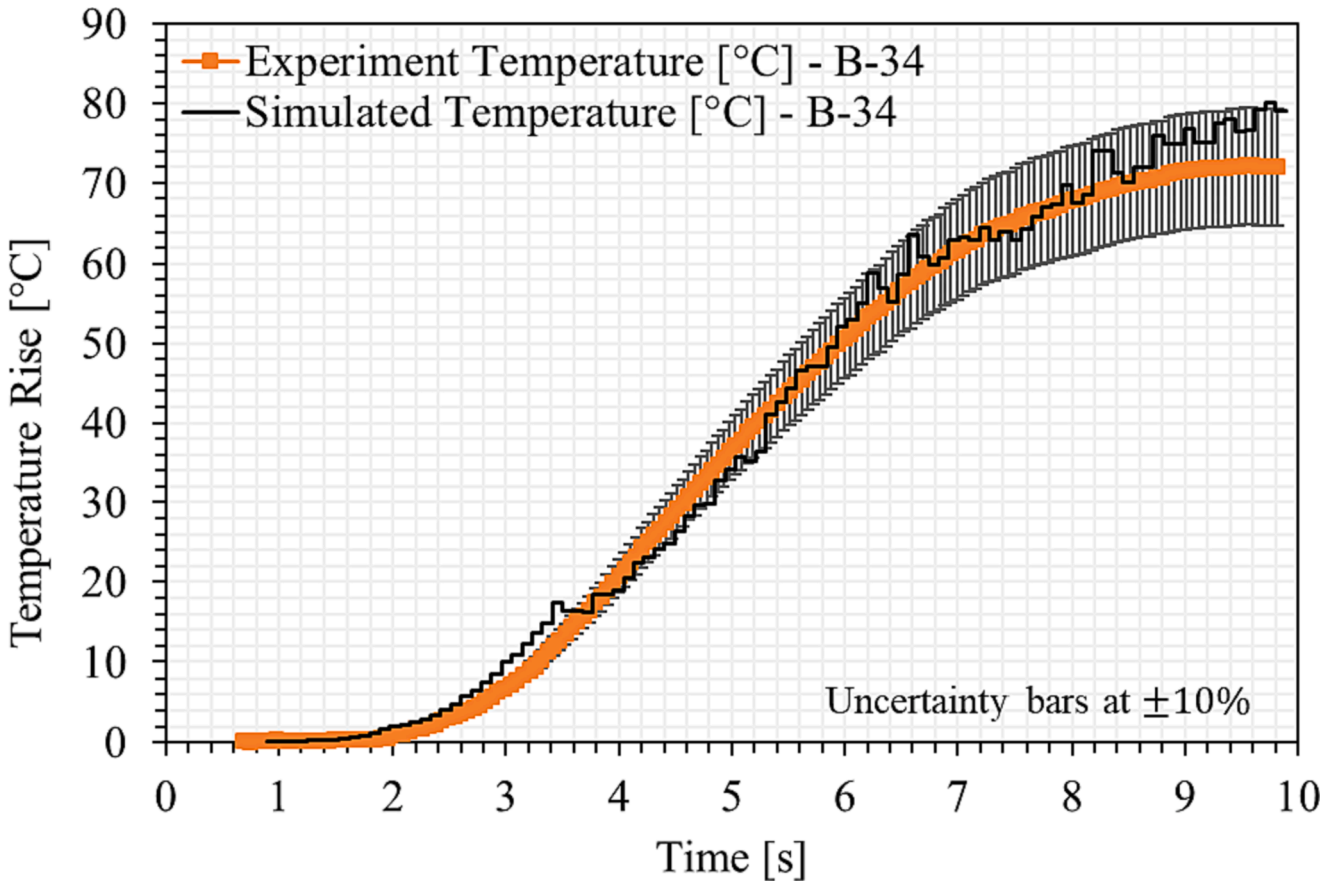

Fig. 21. Comparison of temporal evolution of the cladding temperature between Serpent2/Subchanflow calculation and experimental data for the plate # 136, test B-34.

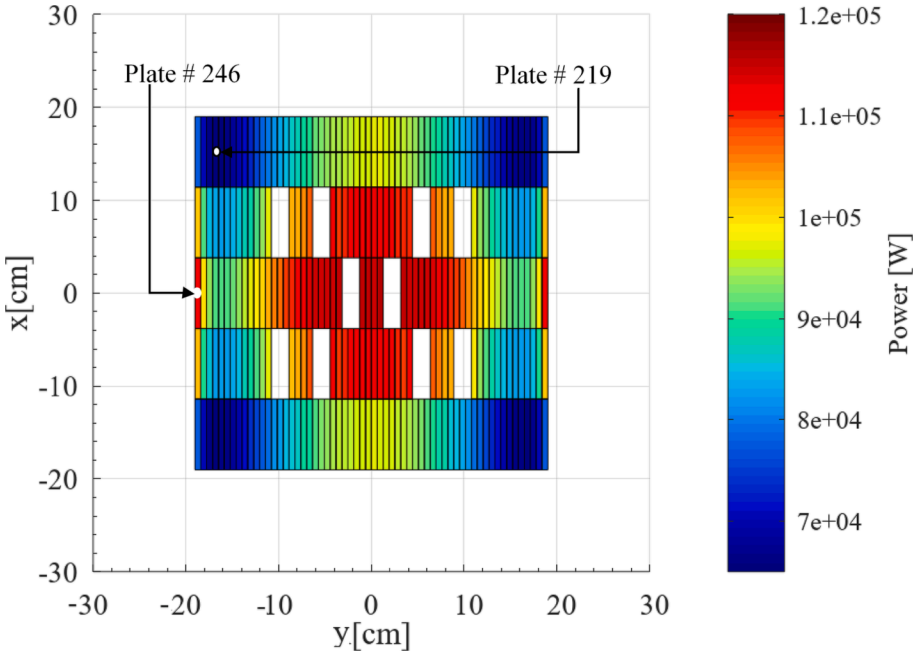

Fig. 22. Radial power distribution for the SPERT IV reactor calculated by Serpent2/Subchanflow, test B-35 at a discrete time of 4.89 s after reactivity insertion.

Finally, Fig. 25 shows the evolution of the measured temperature in the cladding of plate # 136 together with the values calculated by Serpent2/Subchanflow up to a time of 4.89 s. The temperature measurements were made with a thermocouple located at the same coordinates as in test B-34. In test B-35, the maximum temperature measured at t = 4.89 s is 72.26 °C. As it observed Serpent2/Subchanflow

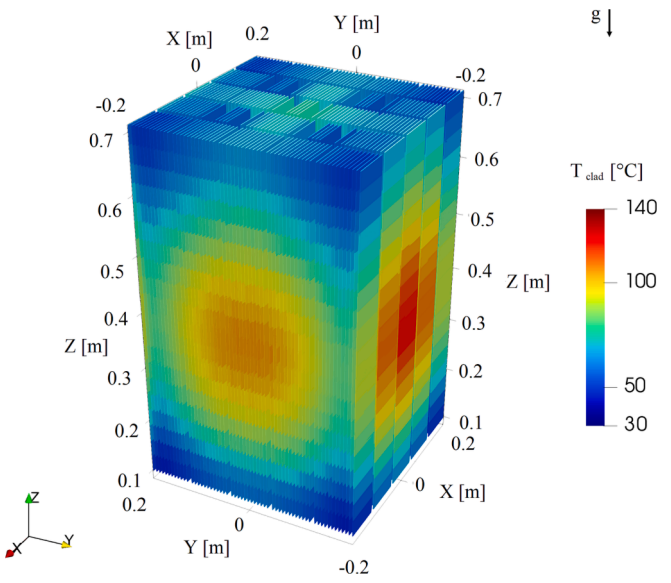

Fig. 23. 3D cladding temperature distribution of reactor SPERT IV D-12/25 test B-35, predicted using Serpent2/Subchanflow at t = 4.89 s.

tends to overestimate and underestimate the cladding temperature values. The overestimation of the calculated data starts to become more pronounced starting at t = 3.2 s and reaching a maximum difference between predicted and measured temperature of 9.36 °C. The overestimation evidenced in plate # 136 may originate from several factors. First, the power recorded in this plate is higher than the average of the rest. In addition, it is important to consider that a uniform radial distribution of the mass flow has been assumed, which could be refined with detailed information of such distribution, possible through computational fluid dynamics (CFD) codes. There is also the possibility that this phenomenon is due to biases in the experimental data. Since this is the first case reported using high-fidelity simulation codes, the assertion of any biases and the need for additional calibrations could be considered after replicating this case with other high-precision codes. However, it should be noted that according to (IAEA, 2015) recommended uncertainty range of ± 10 % for the experimental data, 82 % of the calculated values are in good agreement with the experimental values. These unique results predicted by Serpent2/Subchanflow demonstrate the prediction capability of the coupled Monte Carlo and subchannel code in predicting key-thermal hydraulic parameters at plate/subchannel level never done before for such kind of cores. This validation work of Serpent2/Subchanflow is a very important step for the acceptance and use of such codes as reference solutions for other lower-order solutions i.e. 3D nodal diffusion codes coupled with 1D system thermal hydraulic codes. Of the validation work can be extended for both neutronic and thermal hydraulic parameters if data at plate and subchannel level is available, what is really scarce. For the time-being, it is a very good tool to evaluate the safety features of MTR-reactors compared to the legacy ones in use during the licensing process of such reactors.

5.2.7. *Computer environment for the static and dynamic calculations*

The CPU time used when using the Serpent 2 code was approximately ~ 5 h for each of the proposed positions in Fig. 7. In contrast, the computation time for the static calculations using the coupled Serpent2/Subchanflow code was approximately 8 h for each of the proposed positions in Fig. 12. Both simulations were performed on a cluster with an

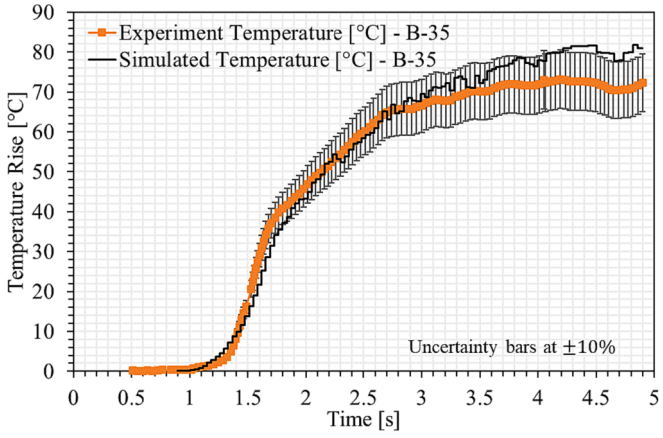

Fig. 25. Comparison of temporal evolution of the cladding temperature between Serpent2/Subchanflow calculation and experimental data for the plate # 136, test B-35.

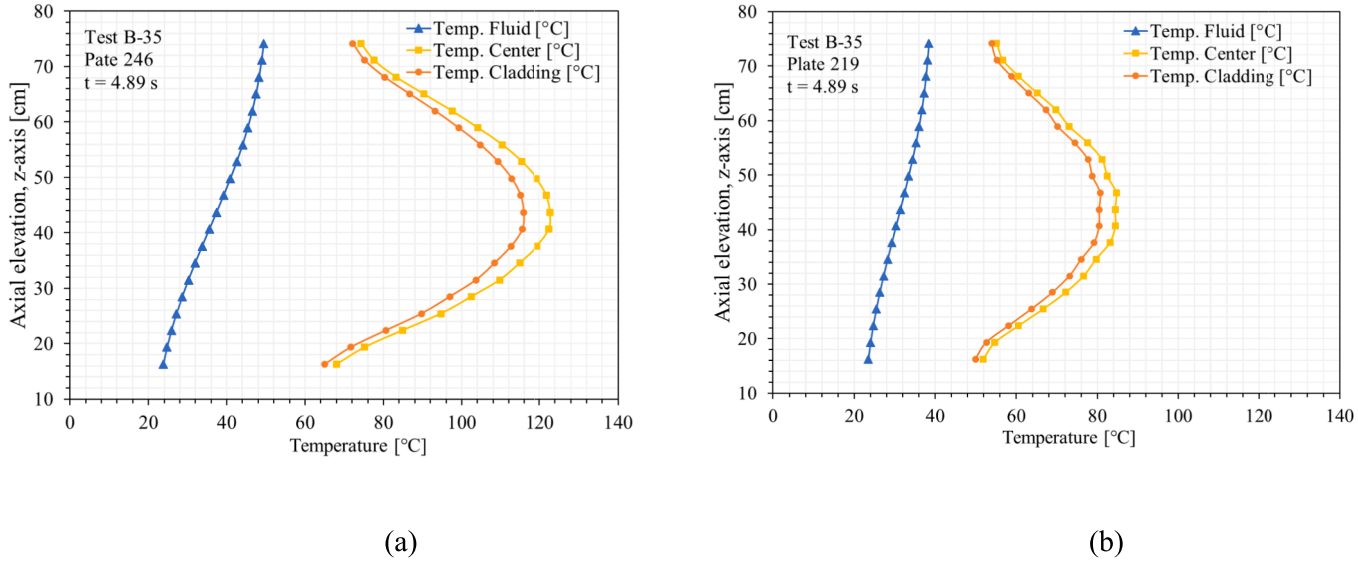

Fig. 24. Test B-35, axial temperature distribution for coolant, cladding and fuel for: (a) maximum power plate # 246; (b) minimum power plate # 219 at t = 4.89 s after reactivity insertion.

Intel(R) Xeon(R) Gold 5118 CPU running at 2.30 GHz on a Debian 4.9.320–2 GNU /Linux system. An OpenMP parallel programming model with 48 CPU (s) was used for these computations.

On the other hand, tests B-34 and B-35 were performed on the HPC HoreKa supercomputer at KIT, equipped with a 2.40 GHz Intel(R) Xeon (R) Platinum 8368 CPU using more than 250 terabytes of main memory. These simulations were run in hybrid mode using 2 MPI nodes and 152 OpenMP cores, resulting in a total of 304 cores per simulation. The runtime for each case was approximately ~ 60 h.

The Serpent 2 code had a lower runtime compared to the coupled Serpent2/Subchanflow coupled code, due to differences in the methods and models implemented. In addition, the use of the HoreKa supercomputer with its powerful hardware allowed more complex and extensive transient simulations to be performed in a reasonable time for tests B-34 and B-35.

5.2.8. Summary and outlook

This study used the high-fidelity Serpent2/Subchanflow code in an MTR reactor, based on assumptions due to the lack of initial parameters. To carry out the transient modeling, assumptions were made on the transient rod motion for reactivity addition to the system. The proposed transient rod velocities and positions are derived from previous calibrations for each of the cases. As this is the first time that these tests are approached, the local thermal–hydraulic results provided should be used for comparison, with results from other low-level codes, considering the lack of uncertainty bands, an aspect that is under progress.

The global transient power values and local plate cladding temperatures calculated by Serpent2/Subchanflow show excellent agreement with experimental data, which represents a significant advance not previously achieved by any other high-fidelity code.

The gain of the detailed plate/subchannel level simulations is that they make it possible to predict key parameters for core safety in a 3D mode, providing information on local thermal–hydraulic and neutronic parameters. This approach allows easy identification and obtaining of axial temperature profiles for high and low power plates, as well as providing temperature profiles for the associated subchannel.

The validation of Serpent2/Subchanflow paves the way for the future use of this code in the safety assessment of MTR-cores in the licensing process of new reactors (e.g. PALLAS). Further validation of the new coupled code for research reactors with other, more complex fuel assembly designs is required and already underway, e.g., for Russian-designed research reactors, which are typically loaded with complex fuel assemblies similar to those of VVR-KN and IRT-4M.

CRediT authorship contribution statement

Juan Carlos Almachi: Conceptualization, Methodology, Software, Writing – original draft. **Victor Sánchez-Espinoza:** Supervision, Project administration, Writing – review & editing. **Uwe Imke:** Conceptualization, Software, Writing – review & editing. **Robert Stieglitz:** Writing – review & editing. **Marat Margulis:** Writing – review & editing.

Declaration of competing interest

The authors declare that they have no known competing financial interests or personal relationships that could have appeared to influence the work reported in this paper.

Data availability

The authors do not have permission to share data.

Acknowledgements

The authors acknowledge the advice of the Serpent team and colleagues especially D. Ferraro and M. Garcia. The financial support of the NUSAFE program at the Karlsruhe Institute of Technology (KIT) and of The Ecuadorian National Secretary for Higher Education, Science, Technology and Innovation (SENESCYT) are highly appreciated. This work was performed on the HoreKa supercomputer funded by the Ministry of Science, Research and the Arts Baden-Württemberg and by the Federal Ministry of Education and Research.

References

Adorni, M., Bousbia-salah, A., D'Auria, F., 2007. Accident analysis in research reactors. In: The International Conference of Nuclear Energy for new Europe. Portoroz, Slovenia. September 10-13, pp 10. ISBN: 978-961-6207-28-7. Retrieved from http://inis.iaea.org/search/search.aspx?orig_q=RN:39095684.

Almachi, J., Sanchez-Espinoza, V., 2022c. Extension of the Validation Basis of Subchanflow by Using Measured Data From the IEA-R1 Research Reactor. Conference: XXXIII Congreso Anual de la Sociedad Nuclear Mexicana, Energía Nuclear: La fuente de energía más eficiente para mitigar el calentamiento globalAt: Mexico-Veracruz, 13. doi:10.5445/IR/1000158402.

Almachi, J., Sanchez-Espinoza, V., 2023. Preliminary validationof Serpent2/Subchanflow using the SPERT IV D-12/25 data. In: European Research Reactor Conference. Antwerp, Belgium. April 12-20. ISBN: 978-92-95064-39-3, pp. 409-419. doi:10.5445/IR/1000158407.

Almachi, J., Sanchez-Espinoza, V., Margulis, M., 2022b. Validation of Serpent 2 using experimental data from the SPERT-IV D-12/25 Research Reactor Tests. In: European Research Reactor Conference of innovative methods in reactor physics and thermohydraulics. Budapest, Hungary. June 6-10. ISBN: 978-92-95064-38-6, pp. 142-150.

Almachi, J., Sánchez-Espinoza, V., Imke, U., 2021. Extension and validation of the SubChanFlow code for the thermo-hydraulic analysis of MTR cores with plate-type fuel assemblies. Nucl. Eng. Des. 379, 111221 https://doi.org/10.1016/j.nucengdes.2021.111221.

Almachi, J., Sánchez-Espinoza, V., Imke, U., 2022a. High-Fidelity Steady-State and Transient Simulations of an MTR Research Reactor Using Serpent2/Subchanflow. Energies 15 (4), 20. https://doi.org/10.3390/en15041554.

Basile, D., Chierici, R., Beghi, M., Salina, E., Brega, E., 1999. COBRA-EN, an Updated Version of the COBRA-3C/MIT Code for Thermal-Hydraulic. Report 1010/1 (revised 1.9.99). Retrieved from https://www.oecd-nea.org/tools/abstract/detail/nea-1614/.

Bousbia-Salah, A., Hamidouche, T., 2005. Analysis of the IAEA research reactor benchmark problem by the RETRAC-PC code. Nucl. Eng. Des. 235 (6), 661–674. https://doi.org/10.1016/j.nucengdes.2004.10.004.

Castellanos-Gonzalez, D., Moreira, J., Maiorino, J., Carajilescov, P., 2018. Validation of the COTENP code: a steady-state thermal-hydraulic analysis code for nuclear reactors with plate type fuel assemblies. Sci. Technol. Nucl. Install. 2018, 17. https://doi.org/10.1155/2018/9874196.

Chadwick, M., Obložinský, P., Herman, M., Greene, N., McKnight, R., Smith, D., Young, P., 2006. ENDF/B-VII.0: Next Generation Evaluated Nuclear Data Library for Nuclear Science and Technology. Nucl. Data Sheets, 107(12), 2931-3060. doi: 10.1016/j.nds.2006.11.001.

Crocker, J., Stephan, L., 1964. Reactor Power Excursion Tests in the SPERT IV Facility. Technical Report IDO-17000, NSA-18-044970, Phillips Petroleum Co. Atomic Energy Div., Idaho Falls, Idaho, USA. doi: 10.2172/4000736.

Crocker, J., Koch, J., Martinson, Z., McGlinsky, A., Stephan, L., 1963. Nuclear Start-up of the SPERT IV Reactor. Technical Report IDO-16905, NSA-17-040407, Phillips Petroleum Co. Atomic Energy Div., Idaho Falls, Idaho, USA. doi: 10.2172/4647654.

Crocker, J., Martinson, Z., Potenza, R., Stephan, L., 1965. Reactor Stability Test in the SPERT IV Facility. Technical Report: IDO-17088, NSA-19-042152, Phillips Petroleum Co. Idaho Falls, Idaho. Atomic Energy Div. USA. doi: 10.2172/4566563.

Daeubler, M., Ivanov, A., Sjenitzer, B., Sanchez, V., Stieglitz, R., Macian-Juan, R., 2015. High-fidelity coupled Monte Carlo neutron transport and thermal-hydraulic simulations using Serpent 2/SUBCHANFLOW. Ann. Nucl. Energy 83, 352–375. https://doi.org/10.1016/j.anucene.2015.03.040.

Doval, A., Villarino, E., Hergenreder, D., Ferraro, D., 2022. INVAP perspectives and initiatives for proliferation resistance as research reactor's designer. In: International Meeting on Reduced Enrichment for Research and Test Reactors. Vienna, Austria. Octuber 3-4, pp. 1-10. Paper ID: S2-P4. Retrieved from https://www.rertr.anl.gov/RERTR42/index.shtml.

Doval, A., 1998. Validation and verification of the MTR_PC thermohidraulic package. In: International Meeting on Reduced Enrichment for Research and Test Reactors, Sao Paulo, Brazil. Octuber 10-23, pp. 1-9. Retrieved from https://www.rertr.anl.gov/Method98/ADoval-abst.html.

Ferraro, D., Garcia, M., Imke, U., Valtavirta, V., Leppänen, J., Sanchez-Espinoza, V., 2019. Serpent/SCF pin-level multiphysics solutions for the VERA Fuel Assembly benchmark. Ann. Nucl. Energy 128, 102–114. https://doi.org/10.1016/j.anucene.2018.12.047.

Ferraro, D., García, M., Valtavirta, V., Imke, U., Tuominen, R., Leppänen, J., Sanchez-Espinoza, V., 2020. Serpent/SUBCHANFLOW pin-by-pin coupled transient calculations for the SPERT-IIIE hot full power tests. Ann. Nucl. Energy 142, 107387. https://doi.org/10.1016/J.ANUCENE.2020.107387.

Ferraro, D., 2021. Monte Carlo-based multi-physics analysis for transients in Light Water Reactors. PhD Thesis, Karlsruhe Institute of Technology, Eggenstein-Leopoldshafen, Germany. McSAFE (EU, H2020, 755097). doi:https://publikationen.bibliothek.kit.edu/1000131803.

Gaheen, M., Abdelaziz, M., 2019. Analysis of natural circulation loop in MTRs using CONVEC code. Prog. Nucl. Energy 117, 103097. https://doi.org/10.1016/j.pnucene.2019.103097.

García, M., Vočka, R., Tuominen, T., Gommlich, A., Leppänen, J., Valtavirta, V., Sanchez-Espinoza, V., 2021. Validation of Serpent-SUBCHANFLOW-TRANSURANUS pin-by-pin burnup calculations using experimental data from the Temelín II VVER-1000 reactor. Nucl. Eng. Technol. 53 https://doi.org/10.1016/j.net.2021.04.023.

Garcia, M., 2021. A high-fidelity multiphysics system for neutronic, thermalhydraulic and fuel-performance analysis of Light Water Reactors. PhD Thesis, Karlsruhe Institute of Technology, Eggenstein-Leopoldshafen, Germany. doi:10.5445/IR/1000140281.

Hainoun, A., Schaffrath, A., 2001. Simulation of subcooled flow instability for high flux research reactors using the extended code ATHLET. Nucl. Eng. Des. 207 (2), 163–180. https://doi.org/10.1016/S0029-5493(00)00410-6.

Heffner, R., Morris, E., Jones, D., Seaman, D., Shane, M., 1962. SPERT IV FACILITY. Technical Repor IDO-16745, NSA-16-014339, Phillips Petroleum Co. Atomic Energy Div., Idaho Falls, Idaho. USA. doi: 10.2172/4785456.

IAEA, 2002. Accident analysis for nuclear power planst. Safety Reports Serie No. 23, International Atomic Energy Agency, Vienna, Austria. ISBN: 92–0–115602–2. Retrieved from https://www.iaea.org/publications/6388/accident-analysis-for-nuclear-power-plants.

IAEA, 2014. Applications of Research Reactors. Series No. NP-T-5.3, INTERNATIONAL ATOMIC ENERGY AGENCY, Vienna, Austria. ISBN: 978–92–0–145010–4. Retrieved from https://www.iaea.org/publications/10491/applications-of-research-reactors.

IAEA, 2015. Research Reactor Benchmarking Database: Facility Specification and Experimental Data. Technical Reports Series No. 480, INTERNATIONAL ATOMIC ENERGY AGENCY, Vienna, Austria. ISBN: 978-92-0-151714-2. Retrieved from https://www.iaea.org/publications/10578/research-reactor-benchmarking-database-facility-specification-and-experimental-data.

IAEA, 2019. Benchmarking Against Experimental Data of Neutronics and Thermohydraulic Computational Methods and Tools for Operation and Safety Analysis of Research Reactors. IAEA-TECDOC-1879, INTERNATIONAL ATOMIC ENERGY AGENCY, Vienna, Austria. ISBN: 978-92-0-109619-7. Retrieved from https://www.iaea.org/publications/13547/benchmarking-against-experimental-data-of-neutronics-and-thermohydraulic-computational-methods-and-tools-for-operation-and-safety-analysis-of-research-reactors.

IAEA, 2022, 12 16. Research Reactor Database. Retrieved from https://nucleus.iaea.org/rrdb/#/home.

Imke, U., Sanchez-Espinoza, V., 2012. Validation of the subchannel code SUBCHANFLOW using the NUPEC PWR tests (PSBT). Sci. Technol. Nucl. Install. 2012, 12. https://doi.org/10.1155/2012/465059.

Labit, J.-M., Seiler, N., Clamens, O., Merle, E., 2021. Thermal-hydraulic two-phase modeling of reactivity-initiated transients with CATHARE2 – Application to SPERT-IV simulation. Nucl. Eng. Des. 381, 111310 https://doi.org/10.1016/j.nucengdes.2021.111310.

Leppänen, J., Viitanen, T., Valtavirta, V., 2012. Multi-physics coupling scheme in the serpent 2 Monte Carlo code. In ANS Annual Winter Meeting 2012. American Nuclear Society, Nov. 11-15, Vol 104, pp 1165-1168,. Retrieved from http://www.fp7-hpmc.eu/papers/conference/ANS-Winter2012_Serpent.pdf.

Leppänen, J., Pusa, M., Viitanen, T., Valtavirta, V., Kaltiaisenaho, T., 2015. The Serpent Monte Carlo code: Status, development and applications in 2013. Ann. Nucl. Energy 82, 142–150. https://doi.org/10.1016/j.anucene.2014.08.024.

Li, L., Zhang, Z., 2010. Development of Real-Time Thermal-Hgydraulic Analysis Code for Plate Type Fuel Reactor. In: The International Conference on Nuclear Engineering, Xi'an, China. May 17–21. Vol 2, pp. 497-505. doi: 10.1115/ICONE18-29297.

Margulis, M., Gilad, E., 2018. Simulations of SPERT-IV D12/15 transient experiments using the system code THERMO-T. Prog. Nucl. Energy 109, 1–11. https://doi.org/10.1016/j.pnucene.2018.07.005.

Motalab, M., Mahmood, M., Khan, M., Badrun, N., Lyric, Z., Altaf, M., 2014. Benchmark analysis of SPERT-IV reactor with Monte Carlo code MVP. Ann. Nucl. Energy 65, 365–369. https://doi.org/10.1016/j.anucene.2013.11.043.

Nogarin, M., 2016. Bolivia: The New Nuclear Research Center in El Alto. Retrieved from atw – Int. J. Nucl. Power 61 (5), 297–300. https://www.kernd.de/kernd-wAssets/docs/fachzeitschrift-atw/2016/atw2016_05_nogarin_nuclear_research_center_el_alto.pdf.

Rohsenow, W., Hartnett, J., Cho, Y., 1998. Handbook of heat transfer. The McGraw-Hill Companies Inc, New York, USA. Retrieved from http://160592857366.free.fr/joe/ebooks/Mechanical%20Engineering%20Books%20Collection/HEAT%20TRANSFER/handbook%20of%20HeatTransfer.pdf.

Schaaf, B., Broekhaus, K., Linden, N., Wijtsma, F., 2011. The Infrastructure for Pallas, the New Nuclear Reactor in the Netherlands. In European Research Reactor Conference, Rome, Italy. ISBN 978-92-95064-11-9, pp. 21-25. Retrieved from http://inis.iaea.org/search/search.aspx?orig_q=RN:42043845.

Sjenitzer, B.L., Hoogenboom, J.E., 2011. A Monte Carlo method for calculation of the dynamic behaviour of nuclear reactors. Progr. Nucl. Sci. Technol., 49(28) 716-721. doi:https://doi.org/10.15669/pnst.2.716.

Sjenitzer, B., 2013. The Dynamic Monte Carlo Method for Transient Analysis of Nuclear Reactors. PhD thesis, Delft University of Technology, Delft, Netherlands. ISBN 978-90-8891-657-1. doi: 10.4233/uuid:6a4bfa4c-2d1f-4648-9698-6eb7ec7e2d11.

Soares, H., Aronne, I., Costa, A., Pereira, C., Veloso, M., 2014. Analysis of Loss of Flow Events on Brazilian Multipurpose Reactor Using the Relap5 Code. Int. J. Nucl. Energy 2014, 12. https://doi.org/10.1155/2014/186189.

Spano, A., Miller, R., 1962. SPERT I Destructive Test Program Safety Analysis Report. Technical Report, NSA-17-001010, IDO-16790, Phillips Petroleum Co. Atomic Energy Div., Idaho Falls, Idaho. USA. doi: 10.2172/4775396.

Sudo, Y., Kaminaga, M., Minazoe, K., 1990. Experimental study on the effects of channel gap size on mixed convection heat transfer characteristics in vertical rectangular channels heated from both sides. Nucl. Eng. Des. 120 (2), 135–146. https://doi.org/10.1016/0029-5493(90)90368-8.

Valtavirta, V., Hessan, M., Leppänen, J., 2016. Delayed Neutron Emission Model for Time Dependent Simulations with the Serpent 2 Monte Carlo Code: First Results. In PHYSOR 2016: Unifying Theory and Experiments in the 21st Century American Nuclear Society (ANS), Sun Valley, USA. May 1-5. ISNS:978-0-89448-762-2, pp. 44. Retrieved from https://cris.vtt.fi/en/publications/delayed-neutron-emission-model-for-time-dependent-simulations-wit.

Viitanen, T., Leppänen, J., 2012. Explicit Treatment of Thermal Motion in Continuous-Energy Monte Carlo Tracking Routines. Nucl. Sci. Eng. 171 (2), 165–173. https://doi.org/10.13182/NSE11-36.

Viitanen, T., Leppänen, J., 2014. Target Motion Sampling Temperature Treatment Technique with Elevated Basis Cross-Section Temperatures. Nucl. Sci. Eng. 177, 77–89. https://doi.org/10.13182/NSE13-37.

Zuccaro-Labellarte, G., Fagerholm, R., 1996. Safeguards at research reactors: Current practices, future directions. Retrieved from Int. Atom. Energy Agency Bull. 38 (4), 20–24. https://www.osti.gov/etdeweb/biblio/458058.